NATIONAL ADVISORY COMMITTEE FOR AERONAUTICS

TECHNICAL NOTE

No. 1257

INVESTIGATIONS OF FREE TURBULENT MIXING

By Hans Wolfgang Liepmann and John Laufer

California Institute of Technology

Washington
August 1947

NATIONAL ADVISORY COMMITTEE FOR AERONAUTICS

TECHNICAL NOTE NO. 1257

INVESTIGATIONS OF FREE TURBULENT MIXING

By Hans Wolfgang Liepmann and John Laufer

SUMMARY

A discussion of the integral relations for flow of the boundary-layer type is presented. It is shown that the characteristic laws of spread of jets, wakes, and so forth, can be obtained directly for the laminar case and, with the help of dimensional reasoning, for the turbulent case as well.

Measurements of the mean velocity, the intensity and scale of the turbulent fluctuations, and of the turbulent shear in a two-dimensional mixing zone are presented. The results of these measurements are compared with the mixing-length theories. It is shown that both mixing length and exchange coefficient vary across the mixing zone. The theories based on the assumption of constant mixing length or exchange coefficient are thus in error.

A discussion of the energy balance of the fluctuating motion is given and the triple correlation is estimated.

INTRODUCTION

The investigations presented herein constitute one part of a long-range research program on the development and nature of turbulent flow. The background and scope of this program are outlined in order to show why the experimental investigations, of which some simple parts were carried out some time ago, should be undertaken.

Theoretical turbulence research can be divided into three main sections: laminar stability, phenomenological theories of fully developed turbulent flow, and statistical theories. Following Reynolds' work, the emphasis of the theoretical research centered mainly on the stability problem. The question of whether laminar flow was stable or not stable in general became the subject of a great many papers. Both the energy method of investigating instability and the method of small perturbations were used extensively. It lies in the nature of these investigations

that they are analytical theories; that is, the results of the stability investigations should lead to results which, without adjusting any constant, agree with experimental findings. The first marked success of the instability theories was G. I. Taylor's discovery of the instability of flow between rotating cylinders which was found to be in excellent agreement with experiment. The theory of stability of two-dimensional flow was first successfully carried through for the case of Couette flow. Results for the more important cases like plane Poiseuille flow and Blasius flow (that is, boundary-layer flow) were doubtful for a long time. The investigations of Heisenberg and Tollmien were not considered mathematically rigorous, and experimental evidence was not available. Only in the last 4 years has the theory of laminar instability been definitely settled as a result of the work of C. C. Lin (reference 1). The results of this instability theory for the Blasius flow were found to be in excellent agreement with experimental results.

The stability theories deal with small perturbations and linearized equations and thus can predict only the lower limit of stability, that is, the limit at which a small perturbation will increase in amplitude for the first time. The stability theories are unable to predict transition and the onset of turbulence. There is little doubt that in both the transition region and the fully developed turbulent region the nonlinear terms are essential, and this is, of course, the reason why an analytical theory of developed turbulence and of transition is nonexistent. Theories of fully developed turbulence are, in general, phenomenological theories. Some problems have also been attacked by statistical methods.

The phenomenological and statistical theories form the second and third groups of theoretical turbulence investigations. The phenomenological theory of turbulent shear flow also goes back to Reynolds' introduction of the "apparent shear." These theories developed very rapidly, following the introduction of the "mixing length" concept by L. Prandtl. The main progress was due to the work of Prandtl, Kármán, and Taylor. The momentum transfer, the vorticity transfer, and the similarity theories were developed in rapid succession. The mean-velocity distributions computed from the mixing-length theories were found to be in good agreement with experimental results at the time. Skin-friction formulas, for example, the famous logarithmic law, could be developed on the basis of these theories and checked with experiments. Experimental research in these years was directed mainly toward finding which of the three main theories was most nearly correct. The answer found from the experimental results, which consisted mainly of measurements of mean-velocity and mean-temperature distributions in boundary layers, channels, jets and wakes, was somewhat disturbing. The flow near a wall was found to agree fairly well with results of the momentum transport and similarity theories; flow in wake and jets agreed better with the vorticity transport theory. The evidence for these various theories has been discussed in reference 2, and in papers by Kármán (reference 3) and Taylor (reference 4). The

shortcomings of these three phenomenological theories have been pointed out clearly by Karman. In the course of the present report, the authors will return to this discussion in some detial.

It is thought that, at the present time, the mixing-length theories have lost much of their value. As a matter of fact, the main results of these theories can be obtained by dimensional reasoning, without the introduction of a hypothesis of the mechanism of turbulence. The mixing length itself, which can now be computed directly from measured quantities, is found to be a complicated function of the coordinates, Thus, the principal advantage of the mixing-length theories, namely the introduction of a "simple" length, is gone. It should be mentioned here that the realization that dimensional analysis furnishes practically all the results of the mixing theories has grown steadily since Kármán's 1937 paper. C. B. Millikan (reference 5), Mises (reference 6), Reichardt (reference 7), and lately Squire (reference 8), have expressed this point of view. In the discussion in later parts of the present report this point will be taken up again.

There remains the third group of theoretical investigations, the statistical approach. In the simplest case, that of isotropic turbulence, first treated by Taylor (reference 9) and subsequently by Kármán (reference 10), a complete kinematic analysis could be developed. The dynamical equations of motion could be reduced to a point at which definite solutions could be obtained for various specific assumptions. But even here there does not exist a physical principle which permits certain selection from among the various possible solutions. There have been but few attempts to extend the statistical theories to more complicated cases such as shear motion; Kármán discussed these possibilities and gave one solution for the case of plane Couette flow. Even more general attempts for a statistical theory of turbulence have been made by Burgers; however, no results which can be checked with experiments have been obtained as yet.

Chou has developed a theory of turbulence (reference 11) using the equations of correlation starting from Reynolds' equation for the double correlation and proceeding to correlations of higher order. Because of the nonlinear term in the equation of motion, it is impossible to obtain an equation which includes only correlations of one order. The double correlation equation thus involves terms containing triple correlation, and so on. The difficulty here is, of course, to find an argument to break the subsequent equations off at a certain point. Here again a clear physical idea is needed, but as yet has not been found. The application of Chou's equation thus involves an arbitrary assumption which, as in previous theories, has then to be checked by a comparison with experimental results.

In summarizing, there exists at the present time no satisfactory theory of turbulent flow. The concept of a simple mixing length is not usable and does not agree with experiment. The recent introduction by Lin, in an unpublished work on velocity and temperature distributions in

turbulent jets, and by Prandtl and Görtler (reference 12) of the assumption of constant exchange coefficient does not agree with measured values of the exchange coefficient, as will be shown in this report. In general, the ability of a specific phenomenological theory to predict a mean-velocity distribution which agrees well with measurements is not at all a proof that the assumptions of the theory are correct. In fact, in the example of the plane mixing region which is discussed in detail in this report, it will be shown that both the theory based on a "constant mixing length" and also the one based on the "constant exchange coefficient" can be made to agree with the experimental mean-velocity distribution, in spite of the fact that neither the measured exchange coefficient nor the measured mixing length is even approximately constant.

The situation, therefore, appears to be as follows: If only the mean-velocity distribution of a turbulent-flow problem is desired, it usually can be obtained by dimensional considerations, assuming a reasonable curve (e.g., an error function in the case of the mixing region), and the determination of one constant from experiment. For an understanding of turbulent flow in general a study of various mean-velocity distributions is of little use. The fields of turbulent fluctuations must be studied in detail. At the present time, it is believed that extensive experimental research is of primary importance. The turbulent fluctuations should be investigated in various cases of turbulent flow ranging from isotropic turbulence to boundary layers and jets. The main purpose of such an investigation would be to determine which characteristics of the fluctuating field are universal and which vary essentially from one group of flow cases to another (e.g., free turbulence like jets and wakes on one hand, boundary layers and channel flow on the other). Reichardt has proposed the development of a theory of turbulence, in an inductive way, from measurements (reference 7). However, since the only basis of Reichardt's approach is mean-velocity distributions, his work is open to exactly the same criticism as that applied to a comparison of other theories with mean-velocity distributions. Reichardt's final equation, therefore, aside from objections which can be raised regarding certain invariant properties, appears to be merely an empirical interpolation formula.

The hot-wire technique is developed to a point at which all fluctuating velocity components and all double correlations can be measured. It is likely that a knowledge of the triple correlation, that is, the diffusion of turbulent energy, is necessary. The development of a hot-wire circuit able to measure triple correlations is at present in progress.

The measurements which are discussed in this report are measurements of flow in a two-dimensional mixing region. Earlier measurements along the same lines of attack have been carried out on an axially symmetrical jet. Measurements in a two-dimensional channel are now in progress as are preliminary measurements of a heated jet with essential differences in density.

To carry out experiments in a field where there is little guidance from the theory is somewhat difficult. It is entirely possible that after a complete theory is known, it will be found that some trivial measurements have been made and important ones omitted. This was the case in the laminar instability and transition investigations in which many measurements of "natural" fluctuations in the laminar layer were carried out by various observers. After the problem was clearly understood, it became evident that many of these measurements were of no use and represented merely investigations of complicated effects related to specific wind tunnels.

In order to reduce this possibility as much as possible, it is necessary to (a) try to define the experimental conditions as clearly as possible; for example, make sure that a "two-dimensional" jet is two-dimensional to a sufficient degree, and (b) use as much guidance as possible from energy and momentum considerations and from dimensional analysis.

In a field as complicated as turbulence, even precautions of this nature are not always successful. For example, the effect of free-stream turbulence upon the isotropic turbulence downstream of a grid has been investigated in three institutions; Cambridge, National Bureau of Standards, and GALCIT, with different results. The reasons for this discrepancy are not yet clear. Here, evidently, a quantity which has been considered of minor importance and has not been measured cannot be neglected. This case shows also that a certain duplication of research is desirable here rather than superfluous.

This investigation was conducted at the Guggenheim Aeronautical Laboratory, California Institute of Technology, under the sponsorship and with the financial assistance of the National Advisory Committee for Aeronautics.

The authors would like to acknowledge the cooperation of Mr. S. Corrsin.

SYMBOLS

x_i Cartesian coordinates. $x_1 \equiv x$ is the longitudinal coordinate; X-axis is defined by the streamline $\frac{u}{U_o} = 0.5$; $x = 0$ corresponds to the jet opening; $x_2 \equiv y$ is the lateral coordinate, increasing toward the free stream

$$\xi = \sigma \frac{y}{x}$$

$$\eta = \frac{y}{b(x)}$$

σ a constant determined by fitting the measured velocity profile to the theoretical one

w magnitude of instantaneous velocity

W magnitude of mean velocity

q magnitude of fluctuating velocity

u_1 component of w in the x_1-direction

$U_1 \equiv u$ component of W in the x_1 ($\equiv x$) direction

$U_2 \equiv v$ component of W in the x_2 ($\equiv y$) direction

u_1' component of q in the x_1-direction ($u_1' \equiv u'$, $u_2' \equiv v'$)

U_o free-stream velocity

p instantaneous static pressure

p' static-pressure fluctuation

ρ density

μ absolute viscosity

υ kinematic viscosity

δ boundary-layer thickness in general

δ^* momentum thickness of boundary layer

λ miscroscale of turbulence

L scale of turbulence

τ shearing stress

ϵ turbulent exchange coefficient

l mixing length

k double correlation coefficient expressing correlation between u' and v' at a given point

R_y double correlation coefficient expressing correlation of u' at two points displaced in y-direction

R_z double correlation coefficient expressing correlation of u' at two points displaced in z-direction

i mean value of current through hot wire

i_o current through hot wire when velocity is zero

e voltage across hot wire

R mean value of resistance of hot wire

R_o resistance of hot wire at 0° C

R_a resistance of hot wire at room temperature

ΔR $R - R_a$

S sensitivity of hot wire to flow perpendicular to wire

Z compensation resistance

γ thermogalvanometer reading

G gain of amplifier

α temperature coefficient of change of resistivity of the hot wire

ANALYTICAL CONSIDERATIONS

Classification of Turbulent-Flow Problems

The fundamental problems in two-dimensional shear flow, turbulent or laminar, can be classified according to the following table:

Boundary	Symmetric	Asymmetric
Free	Jet, wake	Mixing region
Solid	Channel	Boundary layer (Couette flow)

The Couette flow is difficult to realize experimentally. The flow between rotating cylinders is similar, but the influence of centrifugal forces induces secondary flow even in the turbulent case.

The equations of motion for the mean-velocity distribution can be reduced to the standard boundary-layer form of the equations for all these configurations except the channel flow (and also Couette flow), for which even simpler equations hold. It is therefore useful to discuss first the integral relations of boundary flow.

Integral Relations of Boundary-Layer Flow[1]

To discuss the behavior of the mean-velocity distribution, the integral relations for momentum and energy in boundary-layer flow prove very useful. The momentum equations, that is, Kármán's integral equations, have been used a great deal in considerations of this type. It will be seen that the addition of the energy integral equation is very useful for a general discussion of the behavior of the mean velocity distribution. The boundary-layer equations are:

$$\rho u \frac{\partial u}{\partial x} + \rho v \frac{\partial u}{\partial y} = - \frac{\partial p}{\partial x} + \frac{\partial \tau}{\partial y} \tag{1}$$

$$\frac{\partial \rho u}{\partial x} + \frac{\partial \rho v}{\partial y} = 0 \tag{2}$$

Integrating equation (1) with respect to y between two variable limits $a(x)$ and $b(x)$, say, furnishes the momentum integral equation:

$$\int_a^b \rho u \frac{\partial u}{\partial x} \, dy + \int_a^b \rho v \frac{\partial u}{\partial y} \, dy = - (b - a) \frac{\partial p}{\partial x} + \tau_b - \tau_a \tag{3}$$

By transforming the second integral on the left,

$$\int_a^b \rho v \frac{\partial u}{\partial y} \, dy = \left[\rho v u \right]_a^b - \int_a^b u \frac{\partial \rho v}{\partial y} \, dy = \left[\rho v u \right]_a^b + \int_a^b u \frac{\partial \rho u}{\partial x} \, dy$$

Hence, equation (3) becomes:

$$\int_a^b \frac{\partial \rho u^2}{\partial x} \, dy = - \left[b - a \right] \frac{\partial p}{\partial x} + \left[\tau \right]_a^b - \left[\rho u v \right]_a^b \tag{4}$$

[1]It has recently come to the attention of the authors that a generalized technique for the application of integral methods for boundary-layer calculations has been presented by L. G. Loitsianskii in reference 13.

In all cases of free mixing and also for the boundary layer on a flat plate $\frac{\partial p}{\partial x} = 0$, and equation (4) becomes, in the laminar case,

$$\int_a^b \frac{\partial \rho u^2}{\partial x}\, dy = \left[\mu \frac{\partial u}{\partial y} - \rho uv\right]_a^b \tag{5a}$$

and, in the turbulent case,

$$\int_a^b \frac{\partial \rho u^2}{\partial x}\, dy = -\left[\overline{\rho u' v'} + \rho uv\right]_a^b \tag{5b}$$

Equations (5) will be discussed for specific cases after similar equations for the energy have been written.

Multiplying equation (1) with u and integrating furnishes an energy integral equation in the form:

$$\int_a^b \rho u^2 \frac{\partial u}{\partial x}\, dy + \int_a^b \rho uv \frac{\partial u}{\partial y}\, dy = -\frac{\partial p}{\partial x}\int_a^b u\, dy + \int_a^b u \frac{\partial \tau}{\partial y}\, dy \tag{6}$$

By partial integration,

$$\int_a^b \rho uv \frac{\partial u}{\partial y}\, dy = \frac{1}{2}\int_a^b \rho v \frac{\partial u^2}{\partial y}\, dy = \frac{1}{2}\left[\rho u^2 v\right]_a^b - \frac{1}{2}\int_a^b u^2 \frac{\partial(\rho v)}{\partial y}\, dy$$

Therefore,

$$\int_a^b \rho uv \frac{\partial u}{\partial y}\, dy = \frac{1}{2}\left[\rho u^2 v\right]_a^b + \frac{1}{2}\int_a^b u^2 \frac{\partial(\rho u)}{\partial x}\, dy$$

Also,

$$\int_a^b u \frac{\partial \tau}{\partial y}\, dy = \left[u\tau\right]_a^b - \int_a^b \tau \frac{\partial u}{\partial y}\, dy$$

Hence equation (6) becomes:

$$\int_a^b \frac{\partial}{\partial x}\left(\frac{\rho}{2} u^3\right) dy = -\frac{\partial p}{\partial x}\int_a^b u\, dy + \left[u\tau\right]_a^b - \left[\frac{\rho}{2} u^2 v\right]_a^b - \int_a^b \tau \frac{\partial u}{\partial y}\, dy \tag{7}$$

If $\frac{\partial p}{\partial x} = 0$ it follows that, in the laminar case,

$$\int_a^b \frac{\partial}{\partial x}\left(\frac{\rho}{2} u^3\right) dy = \left[\mu u \frac{\partial u}{\partial y} - \frac{\rho}{2} u^2 v\right]_a^b - \int_a^b \mu \left(\frac{\partial u}{\partial y}\right)^2 dy \qquad (8a)$$

and, in the turbulent case,

$$\int_a^b \frac{\partial}{\partial x}\left(\frac{\rho}{2} u^3\right) dy = -\left[\rho u \overline{u'v'} + \frac{\rho}{2} u^2 v\right]_a^b + \int_a^b \rho \overline{u'v'} \frac{\partial u}{\partial y} dy \qquad (8b)$$

The same type of equation can be written for the axially symmetrical case and also for the temperature.

Applications of the Integral Equations

The use of the integral equations for mixing problems will be illustrated by two examples: the jet and the mixing zone.

Jet.- The problem is symmetrical; hence the integration from a to b is replaced by 0 to b(x). Then 2b is taken as the width of the jet, that is, b denotes the distance from the axis of symmetry where, with sufficient accuracy, $u = 0$. Thus, equation (5) becomes,

$$\int_0^b \frac{\partial}{\partial x}(\rho u^2)\, dy = \frac{d}{dx}\int_0^b \rho u^2\, dy = 0$$

Since $\tau = 0$ and $u = 0$ at $y = b$, and $v = 0$ at $y = 0$ by symmetry, equation (8) becomes, similarly,

$$\frac{d}{dx}\int_0^b \frac{\rho}{2} u^3\, dy = -\int_0^b \tau \frac{\partial u}{\partial y}\, dy$$

Hence,

$$\int_0^b \rho u^2\, dy = M = \text{constant} \qquad (9)$$

for both the laminar and turbulent cases and

$$\frac{d}{dx}\int_0^b \frac{\rho}{2} u^3\, dy = \begin{cases} -\int_0^b \mu \left(\frac{\partial u}{\partial y}\right)^2 dy \quad (a) \\ \int_0^b \rho\, \overline{u'v'}\, \frac{\partial u}{\partial y}\, dy \quad (b) \end{cases} \tag{10}$$

In the incompressible, fully developed jet, assume similarity and thus put:

$$u = u_o(x)\, f(\eta) \qquad \eta = \frac{y}{b(x)}$$

Equations (9) and (10a) are sufficient to determine $u_o(x)$, $b(x)$ for the laminar jet. For the turbulent jet an assumption must be made for $\overline{u'v'}$. By dimensional reasoning, let

$$\overline{u'v'} = u_o^2(x)\, g(\eta)$$

Then equation (9) becomes

$$\rho u_o^2 b \int_0^1 f^2(\eta) d\eta = M$$

and equations (10) become

$$\frac{\rho}{2}\frac{du_o^3 b}{dx}\int_0^1 f^3(\eta) d\eta = \begin{cases} -\mu \frac{u_o^2}{b}\int_0^1 [f'(\eta)]^2\, dy \\ \rho u_o^3 \int_0^1 g(\eta)\, f'(\eta)\, dy \end{cases}$$

or, if the constants are omitted for the time being,

$$u_o^2 b \sim \frac{M}{\rho}$$

where ρ = constant over the flow field.

$$\frac{d}{dx}(u_o^3 b) \sim \begin{cases} -\nu \dfrac{u_o^2}{b} & \text{in the laminar case} \\ u_o^3 & \text{in the turbulent case} \end{cases}$$

Hence,

Laminar	Turbulent
$u_o \sim \left(\dfrac{M^2}{\rho^2 \nu\, x}\right)^{1/3}$	$u_o \sim \left(\dfrac{M}{\rho x}\right)^{1/2}$
$b \sim \left(\dfrac{\nu^2 \rho x^2}{M}\right)^{1/3}$	$b \sim x$

Or, if u_i is defined as the initial velocity of the jet, $M = \rho u_i^2$ for a given nozzle size, and the following dimensionless forms can be written:

Laminar	Turbulent
$\dfrac{u_o}{u_i} \sim \left(\dfrac{u_i}{\nu x}\right)^{1/3}$	$\dfrac{u_o}{u_i} \sim \left(\dfrac{1}{x}\right)^{1/2}$
$\dfrac{b}{x} \sim \left(\dfrac{\nu^2}{u_i^2 x}\right)^{1/3}$	$\dfrac{b}{x} = \text{constant}$

The constants can be determined if specific velocity and shear distributions are assumed. For the velocity distribution a reasonable function is, for example,

$$f(\eta) = e^{-\eta^2}$$

Free mixing zone.- In the symmetrical problem of the jet the two integral relations determine the behavior of $u_o(x)$ and of $b(x)$. In the unsymmetrical mixing region there exists a free stream of constant velocity. Similarity downstream means, consequently, that the velocity and shear are functions of only one variable η. Now, however, the mixing process is not symmetrical and two equations are needed to determine the different rates of spread into the free stream and into the air at rest (or into air moving at a different velocity). Call the width of the

region $b(1 + \alpha)$ where b is a function of x, and α is a constant. The momentum-relation, equation (5), furnishes, if $v = 0$ at $y = b$,

$$\int_{-\alpha b}^{b} \frac{\partial \rho u^2}{\partial x} dy = 0$$

or

$$\frac{d}{dx}\int_{-\alpha b}^{b} \rho u^2 dy - \rho U_o \frac{db}{dx} = 0$$

Introducing

$$\eta = \frac{y}{b}$$

$$u = U_o f(\eta)$$

gives

$$\left(\int_{-\alpha}^{1} f^2 \, d\eta - 1\right) \frac{db}{dx} = 0$$

Hence, there is obtained the trivial solution b = constant, that is, no mixing, or

$$\int_{-\alpha}^{1} f^2 \, d\eta = 1$$

which determines α.

The energy equation furnishes:

$$\frac{1}{2}\int_{-\alpha b}^{b} \frac{\partial}{\partial x} (\rho u^3) \, dy = -\int_{-\alpha b}^{b} \tau \frac{\partial u}{\partial y} dy$$

or, with the turbulent $\tau = \rho {U_o}^2 g(\eta)$, since U_o is the only characteristic velocity,

$$\frac{\rho}{2} {U_o}^2 \frac{db}{dx}\left(\int_{-\alpha}^{1} f^3 d\eta - 1\right) = \begin{cases} -\mu \dfrac{{U_o}^2}{b}\displaystyle\int_{-\alpha}^{1} f'^2 \, d\eta & \text{for laminar flow} \\ -\rho {U_o}^3 \displaystyle\int_{-\alpha}^{1} g f' \, d\eta & \text{for turbulent flow} \end{cases}$$

$$\frac{db}{dx}\begin{cases} \sim \dfrac{\nu}{U_o b} & \text{in the laminar case} \\ = \text{constant} & \text{in the turbulent case} \end{cases}$$

$$\frac{b}{x}\begin{cases} \sim \sqrt{\dfrac{\nu}{U_o x}} = \sqrt{\dfrac{1}{R_x}} & \text{in the laminar case} \\ = \text{constant} & \text{in the turbulent case} \end{cases}$$

The different rate of spread is determined once the velocity profile is known.

An extension to the mixing between two streams of different velocities is simple. A suitable velocity profile here is

$$f(\eta) = \phi(\eta)$$

where $\phi(\eta)$ is the error integral. The same function was used by Reichardt (reference 7) and was found to be also the first approximation in Görtler's computations which were based upon the assumption of a constant exchange coefficient (reference 12).

Turbulent mixing problems based on the same assumption have been discussed recently by Squire (reference 8). However, it is believed that the use of an integral relation for the energy as well as for the momentum makes the treatment more uniform and allows the determination of the power laws for velocity and width of mixing zones in a very direct and simple manner.

The Energy Balance for the Fluctuating Motion

A discussion of the energy balance of the fluctuating motion has been given by Kármán (reference 14). The relations given here are essentially the same. Kármán, however, considered parallel shear motion; here it is necessary to deal with flow of the boundary-layer type, that is, in the present case there is no mean-pressure gradient, but there are two components of mean velocity.

In order to derive the equations without extensive writing, it is convenient to change notation and use Cartesian tensor notation to denote the pressure and the components of the velocity:

$$u_1 = U_1 + u_1' \quad p = P + p'$$

$$u_2 = U_2 + u_2'$$

$$u_3 = u_3'$$

Denote the coordinates by x_1, x_2, x_3. Furthermore, the summation convention is applied. The Navier-Stokes equation for incompressible motion can then be written simply as,

$$\frac{\partial u_i}{\partial t} + \frac{\partial u_i u_k}{\partial x_k} = -\frac{1}{\rho}\frac{\partial p}{\partial x_i} + \nu \frac{\partial^2 u_i}{\partial x_j \partial x_j} \tag{11}$$

Equation (11) is written for the instantaneous velocity; averages over time will be taken only after forming an energy equation. This is the essential difference between this equation and the previous energy relation given for the mean flow. Multiplying equation (11) by u_i furnishes

$$\frac{1}{2}\frac{\partial u_i u_i}{\partial t} + \frac{1}{2}\frac{\partial u_i u_i u_k}{\partial x_k} = -\frac{1}{\rho}\frac{\partial p u_i}{\partial x_i} + u_i \nu \frac{\partial^2 u_i}{\partial x_j \partial x_j} \tag{12}$$

Now $u_i u_i = u_1^2 + u_2^2 + u_3^2 = w^2$. Furthermore, the last term on the right side of equation (12) can be rewritten:

$$\nu\, u_i \frac{\partial^2 u_i}{\partial x_j \partial x_j} = \frac{1}{2}\nu \frac{\partial^2 u_i u_i}{\partial x_j \partial x_j} - \nu\left(\frac{\partial u_i}{\partial x_j}\right)\left(\frac{\partial u_i}{\partial x_j}\right)$$

Hence equation (12) becomes

$$\frac{1}{2}\frac{\partial w^2}{\partial t} + \frac{1}{2}\frac{\partial w^2 u}{\partial x_k} = -\frac{1}{\rho}\frac{\partial p u_i}{\partial x_i} + \frac{1}{2}\nu \frac{\partial^2 w^2}{\partial x_j \partial x_j} - \nu\left(\frac{\partial u_i}{\partial x_j}\right)\left(\frac{\partial u_i}{\partial x_j}\right) \tag{13}$$

Now

$$w^2 = U_1^2 + U_2^2 + 2(U_1 u_1' + U_2 u_2') + u_1'^2 + u_2'^2 + u_3'^2$$

$$= W^2 + 2(U_1 u_1' + U_2 u_2') + q^2$$

Take the time average of equation (13), and use the following facts:

(a) The mean motion is assumed steady.

(b) The terms containing only mean-speed terms cancel each other.

(c) The mean value of any fluctuation component vanishes.

There is then obtained

$$\overline{u_1'u_k'}\frac{\partial U_1}{\partial x_k}+\overline{u_2'u_k'}\frac{\partial U_2}{\partial x_k}+\frac{1}{2}\frac{\partial\overline{u_kq^2}}{\partial x_k}=-\frac{1}{\rho}\frac{\partial\overline{p'u_i'}}{\partial x_i}+\frac{1}{2}\nu\frac{\partial^2\overline{q^2}}{\partial x_j\partial x_j}-\nu\overline{\frac{\partial u_i'}{\partial x_j}\frac{\partial u_i'}{\partial x_j}} \quad (14)$$

where

$$\frac{\partial\overline{u_kq^2}}{\partial x_k}=\frac{\partial U_1\overline{q^2}}{\partial x_1}+\frac{\partial U_2\overline{q^2}}{\partial x_2}+\frac{\partial\overline{u_k'q^2}}{\partial x_k}$$

Equation (14) can be simplified somewhat by using the boundary-layer approximations. It must be kept in mind, however, that the boundary-layer conditions apply to the mean speed and the derivatives of mean quantities only, that is,

$$\frac{U_2}{U_1}=O\left(\frac{\delta}{x}\right)$$

if δ denotes a boundary-layer thickness, but

$$\frac{u_2'}{u_1'}=O(1)$$

also,

$$\frac{\partial\overline{q^2}}{\partial x_2}=O\left(\frac{\overline{q^2}}{\delta}\right)\gg\frac{\partial\overline{q^2}}{\partial x_1}$$

however,

$$\frac{\partial u_i'}{\partial x_2}=O\left(\frac{u_i'}{\lambda}\right)=O\left(\frac{\partial u_i'}{\partial x_1}\right)$$

where λ denotes the so-called microscale of turbulence and is discussed in detail later. By using this reasoning, equation (14) becomes:

$$\overline{u_1'u_2'}\frac{\partial U_1}{\partial x_2}+\frac{1}{2}\frac{\partial\overline{u_2'q^2}}{\partial x_2}=-\frac{1}{\rho}\frac{\partial\overline{p'u_2'}}{\partial x_2}+\frac{1}{2}\nu\frac{\partial^2\overline{q^2}}{\partial x_2^2}-\nu\overline{\frac{\partial u_i'}{\partial x_j}\frac{\partial u_i'}{\partial x_j}} \quad (15)$$

The order of magnitude of the terms of equation (15) can now be compared in a way similar to that used in Kármán's paper: the flow represented by

equation (15) contains one characteristic velocity U and two characteristic lengths δ and λ. The fluctuating quantities will, as before, be referred to U. Thus, rewrite: $\overline{q^2} \sim U^2$, and so forth, and the following expression is obtained:

$$a_1 \frac{U^3}{\delta} + a_2 \frac{U^3}{\delta} = - a_3 \frac{U^3}{\delta} + a_4 \nu \frac{U^2}{\delta^2} - a_5 \nu \frac{U^2}{\lambda^2}$$

where the a_i have the character of correlation coefficients and depend on $\frac{x_2}{\delta} = \eta$, say. In comparing the order of magnitude of the terms in equation (15) the following distinction must be made:

(a) Compare the order at a given η, at different downstream positions.

(b) Compare the order at different values of η across the mixing region.

The discussion for item (a) is equivalent to Kármán's discussion.

First,

$$\nu a_4 \frac{U^2}{\delta^2} \ll \nu a_5 \frac{U^2}{\lambda^2}$$

since $\delta \gg \lambda$, and it is very unlikely that a_4 is much different from a_5. The rest of the terms are of the same order if the fundamental relation between λ and δ is satisfied (reference 14), that is, if

$$\frac{\lambda}{\delta} \sim \sqrt{\frac{\nu}{aU\delta}}$$

where a depends on the coefficients a_i and thus $aU \sim q$. That this type of relation is satisfied will be shown later from experimental results in a mixing zone.

To compare the order of magnitude across a mixing zone or boundary layer, as indicated in item (b), requires the knowledge of the mechanism of turbulence or experimental measurements. This corresponds, of course, to the fact that the mean-energy and momentum equations cannot furnish the velocity profile but lead to general relations for the x(downstream) variation of the characteristic quantities after a velocity distribution is known. The general relation is between λ and δ.

From measurements, as reported later, the following picture is obtained:

$\overline{u_1'u_2'}\frac{\partial U_1}{\partial x_2}$	measured ("Production" term)
$\frac{\partial}{\partial x_2}\overline{u_2'q^2}$	unknown ("Diffusion" term involving triple correlation)
$\frac{1}{\rho}\frac{\partial}{\partial x_2}\overline{p'u_2'}$	unknown (same general nature)
$\nu\frac{\partial^2\overline{q^2}}{\partial x_2^2}$	measured
$\nu\overline{\frac{\partial u_i}{\partial x_j}\frac{\partial u_i}{\partial x_j}}$	known approximately (since $\lambda(\eta)$ has been measured)

It is evident from the present considerations that measurement of the triple correlation is extremely desirable. In the following sections of the report a discussion of the measurements for the case of the plane mixing zone is presented. The results of these measurements will then be treated in the light of these considerations.

EQUIPMENT AND PROCEDURE

Wind Tunnel

The investigation was carried out in the wind tunnel shown in figure 1. The tunnel is especially designed for investigations of two-dimensional nature because of an 8:1 aspect ratio (60 by 7.5 in.). The turbulence level is controlled by a honeycomb and seamless precision screens, followed by a 10:1 contraction. The screens have 18 meshes per inch and a wire diameter of 0.018 inch. The honeycomb consists of paper mailing tubes, 6 inches long and 1 inch in diameter.

The jet emerging from the contraction (fig. 1) is allowed to mix on one of its boundaries with the still air. The other boundaries are solid walls. It is especially important that the boundary opposite to the mixing zone under investigation be closed. This is achieved by means of a plate-glass surface which reduces influences of any draft in the room on the half jet and improves the two-dimensional character of the jet.

The tunnel is operated by a 62-horsepower stationary natural-gas engine, normally operating at a fraction of its rating, which drives two eight-blade fans. The speed is controlled remotely by means of a small electric motor which drives the throttle through a gear and lead-screw system. The velocity range of the tunnel is about 5 to 40 meters per second. The experiments were carried out at a speed of 18 meters per second.

Traversing Mechanism

Figures 2, 3, and 4 show the types of mechanism used during the experiments. Traversing in the longitudinal direction (x-direction), parallel to the mean flow, was done by a hand-operated screw (fig. 2). In the lateral direction (y-direction) the hot-wire carriage was moved by a small 6-volt direct-current motor (fig. 3). A revolution counter indicated the position of the hot wire within ±0.02 centimeter.

The hot-wire carriage (fig. 3) consisted of a Z-shape brass bar which could be rotated in a horizontal plane by means of a small gear and lead-screw system. Means were provided for reading the rotation angle. The hot-wire holder consisted of ceramic tubing fitted in a short brass tube mounted on the top of the Z bar. The mounting was so constructed that the hot-wire holder could be rotated in horizontal and vertical planes. This arrangement was necessary for measurements of v' and correlation coefficient k.

For the measurements of the R_y correlation, the traversing mechanism shown in figure 4 was used. One of the hot-wire holders was stationary, the other was movable by means of a hand-operated screw. Care was taken to maintain the two hot wires parallel. The initial distance between the wires was measured with an ocular micrometer. The accuracy of the mechanism was ±0.006 centimeter.

Hot-Wire Equipment

The hot-wire apparatus used during the measurements is described in detail in reference 5.

Mean-speed measurements.- A half-mil (0.0005 in.) platinum wire of 1-centimeter length was used. The measurements were made by the constant-resistance method. This method has the advantage of keeping the wire sensitivity constant throughout the velocity profile.

It must be kept in mind, of course, that the hot wire measures the absolute magnitude of the velocity. However, as will be seen later, it is justifiable to assume that the lateral component of velocity is very much smaller than the longitudinal component throughout the main portion of the half jet.

The transverse component of the velocity was also measured at $x = 54.3$ centimeters. The method was as follows: Two identical hot wires were placed at a distance of 15 centimeters, one behind the other in the downstream direction. The velocity difference Δu was measured across the mixing zone. Since

$$\frac{\Delta u}{\Delta x} \approx \frac{\partial u}{\partial x} = -\frac{\partial v}{\partial y}$$

the graphical integration of the function

$$\frac{\partial v}{\partial y} = f(y)$$

gives the distribution of the transverse component of the velocity for a constant value of x.

Turbulence measurement.- For the investigation of turbulent fluctuations, 0.00024-inch Wollaston wire was used. The wire was soft-soldered to the tips of fine sewing needles after the silver coating had been etched off. The longitudinal component of the fluctuations was measured with a single hot wire, the lateral component with a bi-plane X-type meter composed of two hot wires. The measurements were carried out by conventional methods.

Measurement of the double correlation coefficient $\frac{\overline{u'v'}}{\sqrt{u'^2}\sqrt{v'^2}}$.- The method used is similar to the one proposed by H. K. Skramstad (reference 16). The correlation coefficient was measured with the same X-type meter as was used for v' measurements. The method consists in putting the outputs of the two wires separately through the amplifier, and also the sum (or difference) of the outputs. It is essential to make a correction for the difference in sensitivity of the two wires. The method of correction is given in appendix A. This method was worked out and used by P. Johnson at the California Institute of Technology during similar measurements on a flat plate.

An alternative method of measuring the double correlation coefficient was also used; this involved photographic recordings of correlation figures from the screen of an oscilloscope. This type of measurement was first made by Reichardt (reference 7). The procedure is as follows: u'- and v'-meters are mounted next to each other as close as possible. The signals from the meters are amplified by two separate amplifiers which must, of course, have the same frequency and phase-shift characteristics. The separate outputs of the two amplifiers are then connected, one to the horizontal and the other to the vertical deflection plate of the oscilloscope. The gain of the oscilloscope amplifiers is set in such a way that the amplitudes of the horizontal and vertical fluctuations

become the same. The crosses on the pictures (figs. 5 to 11) are obtained by setting the gain of first the horizontal and then the vertical oscilloscope amplifier to zero; thus a check for the amplitudes of the fluctuations is obtained. The figures were photographed with an exposure time of 15 seconds. The correlation coefficient is calculated from the equation

$$k = -\frac{a^2 - b^2}{a^2 + b^2}$$

where a and b are the major and minor axes, respectively, of the correlation ellipse.

Measurement of microscale turbulence.- This involved measurements of correlation between longitudinal velocity fluctuations at two different points. Two parallel 0.00024-inch wires were used, one stationary and one movable. From the outputs of the wires, R_y was computed. The microscale of turbulence then was obtained by fitting a parabola to the upper part of the R_y correlation curve.

Correlation figures were also obtained on the screen of an oscilloscope.

RESULTS AND DISCUSSION

Velocity Distributions

Careful velocity measurements and visual observation of the velocity fluctuations on the oscilloscope show the following facts:

(a) The boundary layer at the mouth of the jet is only 0.1 centimeter thick and is laminar.

(b) The free boundary layer is laminar from $x = 0$ to $x \doteq 6$ centimeters. The transition from laminar to turbulent flow at $x \doteq 6$ centimeters can be seen clearly on the oscilloscope.

(c) Fully developed turbulent-velocity profiles are obtained only for $x > 30$ centimeters, approximately.

Figure 12 shows the mean-velocity distributions across the mixing zone at different stations downstream: at $x = 10$, 30, 54.3, 75, and 90 centimeters. For convenience in the figure the x-axis is chosen parallel to the free-stream direction. (This is Tollmien's notation; in all other figures the x-axis corresponds to the $\frac{u}{U_o} = 0.5$ streamline.) The

boundaries of the mixing region were chosen arbitrarily, defined by the streamlines corresponding to $\frac{u}{U_o} = 0.95$ and $\frac{u}{U_o} = 0.10$. It can be seen that for $x > 30$ centimeters, where the fully developed turbulent velocity profiles exist, the spread is linear.

In order to demonstrate more explicitly the difference between the velocity distributions in the partially developed and the fully developed turbulent mixing regions, figure 13 shows the measured velocity profiles plotted on a nondimensional scale. It is immediately obvious that while the velocity profiles measured at $x = 90$, 75, 65, and 54.3 centimeters (the fully developed region) follow the same curve, that is, they are similar; at $x = 20$ the measured profile deviates appreciably from the fully developed type.

The results of the lateral-velocity-component measurements are given in figure 14. The measurements were carried out only up to $\xi = -0.6$, because at larger values of ξ the front hot wire was in the region where u is no longer large compared with v; therefore, the assumption that the absolute magnitude of the velocity indicated by the hot wire may be considered equal to the velocity component, u, no longer holds.

By use of Görtler's theoretical values of the lateral mean-velocity component, which are convenient and accurate enough for computing a correction of this type, u/U_o was calculated from the measured absolute magnitude of the velocity. It was found that, in the region $\infty < \xi < -1.4$ the error involved in neglecting this correction is of the same order of magnitude as the experimental scatter. This justifies neglecting the difference between the absolute magnitude of the velocity and its longitudinal component for $\infty < \xi < -1.4$, and the hot-wire measurements may be considered to be correct in this region.

One mean-velocity distribution, that at $x = 54.3$ centimeters, was measured with a total-head tube in order to see how closely the results agreed with the hot-wire measurements. The results are plotted in figure 17; the agreement seems to be satisfactory. The effect of large velocity fluctuations on the high total-head-tube reading at low velocities can be seen clearly in the figure.

On comparing the results with measurements given in the papers of Tollmien (reference 18) and Cordes, the agreement seems to be satisfactory; Reichardt's results, however, diverge appreciably. The value of σ $\left(\sigma \equiv \frac{1}{3\sqrt{2c^2}} \text{ in Tollmien's notation} \right)$ obtained by the Göttingen measurements (reference 19) is 11.99; Cordes gives $\sigma = 11.95$ (reference 15) as compared with 12.0 obtained with the present measurements (fig. 14), in

each case the value of σ being chosen for the best fit to Tollmien's curve. Fitting Görtler's theoretical curve the present measurements give $\sigma = 11.0$ (fig. 15); while Reichardt's value of σ is 13.5 (reference 12). Reichardt noticed the discrepancy between his and earlier measurements and explained it by the fact that early measurements did not go far enough away from the jet opening. It is believed, however, that three-dimensional effects may have disturbed the flow conditions during Reichardt's measurements. The two-dimensionality of the jet used during the present measurements was checked and confirmed.

In a comparison of the measured velocity profiles with the existing theories it was found, as mentioned in the Introduction, that by an appropriate choice of the constant σ both the theory based on constant mixing length and the one based on constant exchange coefficient can be made to agree with the velocity distribution obtained by measurement. Figure 14 shows that for $\sigma = 12.0$ the agreement with Tollmien's velocity profile is fairly good; while for $\sigma = 11.0$ Görtler's velocity profile is better approximated (fig. 15). As a matter of fact, an error integral curve (Görtler's first approximation) gives a reasonable agreement with the measured values as shown in figure 14.

In order to avoid this arbitrariness in the choice of σ, a convenient parameter was chosen that could be completely defined from the measured velocity distributions at every value of x. Such a parameter is ϑ, known as the momentum thickness in the boundary-layer theory, and is defined at a given value of x as (for Const Density)

$$\vartheta = \int_{-\infty}^{\infty} \frac{u}{U_o}\left(1 - \frac{u}{U_o}\right) dy$$

Therefore, in presenting the measured data in the figures subsequent to figure 15, all quantities are plotted against y/ϑ.

Turbulence Level

Measurements of the longitudinal and lateral components of the velocity fluctuations were carried out at three stations: $x = 30$ centimeters, $x = 54.3$ centimeters, and $x = 75$ centimeters. Figures 16, 17, and 18 show the distribution of the relative velocity fluctuations or turbulence levels, u'/u and v'/u, at the three stations. It can be seen from these figures that

(a) The lateral distribution of u'/u remains very nearly the same for different distances downstream of the jet opening; the same is true of v'/u.

(b) Both turbulence levels reach a maximum at the outer edge of the mixing zone.

It is interesting to note that Corrsin's measurements in an axially symmetrical jet (reference 20) show similar distributions of both u'/u and v'/u. Of course, the turbulence levels in the high-velocity region of each cross section are much higher because a fully developed free-turbulent jet has no free-stream flow; that is, it has no adjacent stream with $\frac{\partial u}{dy} = 0$ and with a turbulence level which is small and due to the tunnel only and hence, independent of the mixing mechanism. Nevertheless, the general character of the distributions is similar in the two cases.

In order to get a better picture of the velocity fluctuations themselves, u' and v', their distribution is plotted in a dimensionless form, u'/U_o and v'/U_o, in figure 19. It is seen that the value of u'/U_o is considerably higher across the mixing zone than the value of v'/U_o. Furthermore, the v' fluctuations seem to reach maximum value somewhat closer to the free stream than do the u' fluctuations. Also it should be noted that the fluctuations are somewhat lower for $x = 30$ centimeters, because the region here has not yet reached the fully developed turbulent state.

It should be mentioned that no effort was made to correct the hot-wire measurements in regions of high turbulence level. The nature of these corrections is discussed briefly in reference 20.

Correlation Coefficient Measurements

Figures 16, 17, and 18 show the distribution of the double correlation coefficient $k = \frac{\overline{u'v'}}{u'v'}$ at the stations $x = 30$ centimeters, $x = 54.3$ centimeters, and $x = 75$ centimeters. A comparison of the three distributions is given in figure 19 where the solid line indicates the average values of the correlation coefficient at the three stations.

The correlation coefficients on the free-stream side of the mixing zone seem to be somewhat high. This probably is due to the fact that the measurement of the wire sensitivities S_1 and S_2 is more difficult here because of the one-sided fluctuations, which will be mentioned later. Furthermore, the influence of the ratio S_1/S_2 on the value of k is more pronounced in this region (appendix A).

As mentioned earlier, an alternative method of measuring the correlation coefficient was also employed. These measurements, however, are less accurate. This becomes particularly evident near the free stream

(figs. 6 and 7). It can be seen that calculation of the correlation coefficient (that is, by measuring the major and minor axes of the "ellipse") from figures 6 and 7 is unreliable. From figures 9 and 10 the calculated correlation coefficient is $k = -0.45$, and $k = -0.38$ as compared with $k = -0.51$ and $k = -0.40$ obtained by using the double hot-wire method. On the other hand, the pictures show the interesting way in which the correlation between u' and v' changes across the mixing zone. Figure 5 is taken in the free stream where $k = 0$. It is worth noticing that the circular spot is formed by individual arcs of more or less circular shape. This can be seen even better in figure 20, where on the right side a picture of short exposure shows the shape of such an arc. This shows that although $k = 0$ in the free stream, the fluctuations in the free stream are not entirely of random character, which is a well-known characteristic of low-turbulence tunnels. The picture in figure 21 was taken in the isotropic turbulent field behind a screen. Again $k = 0$, but the picture on the right shows that here u' and v' are truly of random character.

Figure 6 was taken at the free-stream edge of the mixing zone. It is seen that the circular shape of the correlation figure is somewhat distorted, an indication that the correlation coefficient is no longer zero. It is to be noted that this distortion occurs in only one direction. In figures 7 and 8 the distortion is even more pronounced. Figure 9 shows the highest correlation; while figures 10 and 11 were taken on the outer edge of the mixing zone (that is, the zero-velocity edge) where the correlation coefficient decreases.

Corrsin (reference 20) also measured the correlation coefficient at one section in the axially symmetrical jet. The maximum value was -0.42. The explanation for the difference between that maximum value and the one presented here is not evident.

Turbulent Shearing Stress

From the measured correlation coefficient and the components of the turbulent fluctuations, the turbulent shear can be calculated easily.

Figure 22 shows a comparison of the measured shear and that obtained from Tollmien's and Görtler's theories. The method of computing the shear distributions from the velocity profile of Görtler was given by C. C. Lin (appendix B). The same method was used for calculating the shear from Tollmien's velocity profile; of course, this can be carried out analytically since the velocity distribution is given in a closed form.

It is seen that the measured shear is considerably smaller than the theoretical values of Tollmien and Görtler. The difference between the maximum values is about 25 percent. The difference on the outer edge of

the mixing zone is even larger and is, of course, due to the fact that both theories assumed fully turbulent flow across the entire width of the mixing zone. This assumption was found to be incorrect. (See oscillograms in reference 20.)

The calculation of the shear distribution from the measured velocity profile was also carried out. In evaluating the constant of integration (appendix B) the condition that τ be maximum where $\frac{\partial^2 u}{\partial y^2} = 0$ was used instead of the boundary condition at the outer edge of the mixing region; that is, $\tau = 0$ when $\frac{\partial u}{\partial y} = 0$.

The reason for choosing this was that at the outer edge of the mixing region the simplified form of the flow equation used in the analysis does not hold; it was thought, therefore, that the evaluation of the constant of integration from conditions at the outer edge is not justified. The condition that τ has a maximum at $\frac{\partial^2 u}{\partial y^2} = 0$ appears physically sound. (The mixing-length theories lead also, of course, to this condition.) It should be pointed out that by this method of calculation the shear has positive values at the outer edge of the mixing zone.

Figure 22 shows a good agreement between the calculated shear from the measured velocity profile and the measured shear.

From the measured shear and the velocity gradient, the mixing length and the exchange coefficient distributions across the mixing zone were computed (fig. 23). The irregular shape of the curves is due to the difficulty of obtaining the slope of the velocity profile graphically.

It is seen from figure 23 that neither the assumption of constant mixing length nor that of constant exchange coefficient holds throughout the mixing region.

Microscale of Turbulence

Measurements of correlation between the longitudinal fluctuations at two different points at various positions in the mixing region are presented in figures 24 to 29. The measured values of R_y were plotted on a rather large scale, so that the parabola defining the microscale of turbulence λ could be obtained with reasonable accuracy. Figure 24 shows the R_y distribution at different lateral positions for $x = 30$ centimeters. It is seen from this figure that the parabola corresponding

to $\lambda = 0.24$ centimeter is fairly well defined by the measured points and that the parabolas corresponding to $\lambda = 0.21$ centimeter and $\lambda = 0.27$ centimeter fall above and below the measured points, respectively. Thus the determination of λ by fitting the R_y curve in the neighborhood of the origin can be obtained within about 10 percent accuracy.

Figure 24 is reproduced in figure 25 in order to show more explicitly the interesting result that the microscale of turbulence is constant across the mixing region. This result is confirmed further by measurements at the cross sections $x = 54.3$ centimeters and $x = 75$ centimeters (figs. 27 and 28).

Considerable error in measurements was introduced at points close to the outer edge of the mixing zone. At these points, the large lateral component of the velocity caused the outer wire to fall into the wake of the inner one as the two wires were placed close to each other. Figure 30 shows this effect. It is seen that, while for $\frac{y}{\vartheta} = -0.97$ the effect shows up only when the wires are 0.025 centimeter apart, for $\frac{y}{\vartheta} = -3.48$, the error becomes appreciable at a wire distance of 0.10 centimeter. No effort was made to correct such error; measurements at such points were disregarded since any correction at these large turbulent levels is doubtful.

As a matter of interest, some correlation pictures were taken at the point $x = 75$ centimeters, $\frac{y}{\vartheta} = 1.99$ for wire distances $d = 0.027$, and $d = 0.192$ centimeter. (See figs. 31 and 32.) The pictures on the left-hand side were taken with a 15-centimeter exposure, the ones on the right were instantaneous pictures. The calculated correlation coefficients from these pictures are $R_y = 0.985$ and $R_y = 0.89$ as compared with 0.990 and 0.902 obtained by direct measurements.

The correlation coefficient R_z, expressing the correlation between the u' fluctuations at two points displaced in the z-direction, was also measured at one point of the mixing zone to check the assumption of two-dimensional flow. Figure 33 shows that the R_y and R_z distributions are identical within the range of scatter.

Scale of Turbulence

From the measured R_y distributions, the magnitude of the scale of turbulence could be estimated. This was done by fitting an exponential

function to the R_y distribution, as shown in figure 34. It was found that for a given value of x the scale decreases somewhat from the free-stream side of the mixing region toward the outer edge. The longitudinal distribution of the scale at approximately the same values of y/ϑ shows a linear increase with x. (See fig. 35.) This figure also shows the variation of the microscale of turbulence with x. This variation can be approximated by a parabola (straight-line approximation would give a finite value of $x = 0$).

Energy Balance Estimated from the Measured Quantities

The energy equation in a two-dimensional mixing region has the form (from equation (15) under Analytical Considerations):

$$\frac{\tau}{\rho}\frac{\partial u}{\partial x_2} - \frac{\partial}{\partial x_2}\left[\overline{u_2'\left(\frac{q^2}{2} + \frac{p'}{\rho}\right)}\right] + \frac{1}{2}\nu\,\overline{\frac{\partial^2 q^2}{\partial x_2^2}} - \nu\,\overline{\frac{\partial u_i'}{\partial x_j}\frac{\partial u_i'}{\partial x_j}}$$

The first term represents the production of turbulent energy and can be calculated from the measured shear stress and velocity profile. The third term can also be calculated from the measured fluctuating velocities and can be shown to be negligibly small compared with the other quantities. The fourth term represents the energy dissipation due to viscosity. The magnitude of this quantity can be approximated from the measured microscale of turbulence. Each term of the dissipation

$$D = \nu\,\overline{\frac{\partial u_i'}{\partial x_j}\frac{\partial u_i'}{\partial x_j}}$$

can be expressed in terms of a microscale. If the turbulence is isotropic, the dissipation can be written in terms of a single microscale λ:

$$D = 15\,\nu\,\frac{u'^2}{\lambda^2} \qquad \text{(reference 9)}$$

λ being a function of R_y. During the present measurements, only this λ was measured, and although the turbulence in the mixing region is not isotropic, as a first approximation the dissipation was calculated from the foregoing relation.

Figure 36 shows the turbulent energy production and dissipation as a function of y/ϑ. The difference of the two function gives, according to the energy equation, the diffusion term. It is interesting to notice that all three energy terms reach their maximum value at about the same region, namely, close to the inflection point of the velocity distribution.

From the diffusion term, the distribution of the energy transport through a unit surface can be estimated. It is seen from figure 37 that, in the middle of the mixing region, this term is small compared with the double correlation coefficient and becomes gradually larger on approaching the two edges of the mixing region. At the edges, however, no conclusive remarks can be made as to the relative magnitude of the triple correlation, since all simplified assumptions made in the evaluation of the diffusion term fail there.

CONCLUSIONS

Measurements of the field of fluctuating velocities in a turbulent mixing zone show that both the mixing length and exchange coefficient vary across the mixing region. The theories of Tollmien and Prandtl-Görtler which assume constant mixing length and constant exchange coefficient, respectively, are thus based on invalid assumptions. It is typical of phenomenological theories of turbulence that the mean-speed distributions derived from such theories can be brought into fair agreement with experimental measurements. This is found to be the case here also if the results of Tollmien and Prandtl-Görtler velocity distributions are compared with the measured distributions. Conclusions regarding the physical significance of theories of turbulence must be based on comparison with experimental investigations of the field of fluctuating velocities.

The discussion of the energy and momentum integral relations for the mean and fluctuating motion shows that the over-all characteristics of a turbulent mixing process can be obtained by dimensional reasoning without any assumptions for the physical mechanism of turbulent motion.

The following results of the measurements of turbulent field appear of general importance:

(a) The microscale of turbulence λ was found to be constant across the larger part of the mixing zone.

(b) Kármán's fundamental relation between λ and the scale of turbulence L was found to hold.

(c) The double correlation coefficient reaches a maximum value of approximately -0.55 near the inflection point of the mean-velocity distribution.

(d) The three energy terms - production, diffusion, and dissipation of energy - are found to have a maximum value in the middle of the mixing region.

Guggenheim Aeronautical Laboratory,
California Institute of Technology
Pasadena, Calif., July 24, 1946

APPENDIX A

METHOD OF CORRECTION FOR THE DIFFERENCE IN SENSITIVITY OF TWO HOT WIRES USED FOR CORRELATION-COEFFICIENT MEASUREMENTS

The equilibrium equation of the hot wire is given in the form (reference 21)

$$\frac{\alpha i^2 R R_o}{\Delta R} = A' + B' \sqrt{u}$$

where A' and B' are constants.

With $$A = \frac{A'}{\alpha R_o} \quad \text{and} \quad B = \frac{A'}{\alpha R_o}$$

the equation becomes

$$\frac{i^2 R}{\Delta R} = A + B \sqrt{u} \tag{1}$$

With i constant the differential of equation (1) is

$$-\frac{i^2 R_a}{(\Delta R)^2} dR = \frac{1}{2} B \sqrt{u} \frac{du}{u}$$

$$= \frac{1}{2}\left(\frac{i^2 R}{\Delta R} - A\right)\frac{du}{u}$$

$$= \frac{1}{2}\frac{R}{\Delta R}\left(i^2 - i_o^2\right)\frac{du}{u}$$

since $i_o^2 = \frac{A \Delta R}{R}$ by definition

or

$$\frac{du}{u} = \frac{2 R_a i^2 \, dR}{\Delta R R (i^2 - i_o^2)}$$

Let $e = i d R$ and $S(i_1 R)$ = wire sensitivity $= \frac{R \Delta R (i^2 - i_o^2)}{i R_a}$

then

$$\frac{du}{u} = \frac{2e}{S} \tag{2}$$

On impressing the voltage e across the amplifier input the thermogalvanometer reading will be

$$\overline{e^2} = G^2\frac{\gamma}{Z^2} = D^2\gamma \tag{3}$$

where

$$D = \frac{G}{Z}$$

If U is considered as the component of the mean velocity perpendicular to the hot wire, and the effect of the flow parallel to the wire is neglected, the equations for uniform, unsteady flow across two wires, as shown, are found in the following manner:

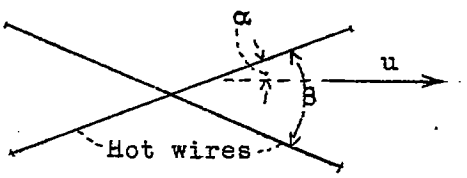

$U_1 = u \sin \alpha$

$dU_1 = \sin \alpha \, du + u \cos \alpha \, d\alpha$

Let $du = u'$, and $u \, d\alpha = v'$

$$\left.\begin{aligned} dU_1 &= u' \sin \alpha + v' \cos \alpha \\ \frac{dU_1}{U_1} &= \frac{u'}{u} + \frac{v'}{u} \cot \alpha \\ U_2 &= u \sin (\beta - \alpha) \\ dU_2 &= \sin (\beta - \alpha) \, du - u \cos (\beta - \alpha) d\alpha \\ &= u' \sin (\beta - \alpha) - v' \cos (\beta - \alpha) \end{aligned}\right\} \tag{4}$$

$$\frac{dU_2}{U_2} = \frac{u'}{u} - \frac{v'}{u} \cot (\beta - \alpha)$$

or for the case $\beta = 2\alpha$,

$$\frac{dU_2}{U_2} = \frac{u'}{u} - \frac{v'}{u} \cot \alpha \tag{5}$$

For the case $\alpha = 45^\circ$, equations (4) and (5) become

$$\frac{dU_1}{U_1} = \frac{u'}{u} + \frac{v'}{u} \tag{6a}$$

$$\frac{dU_2}{U_2} = \frac{u'}{u} - \frac{v'}{u} \tag{6b}$$

From equations (2) and (6a),

$$\overline{e_1^2} = \frac{S_1^2}{4}\left[\overline{\left(\frac{u'}{u}\right)^2} + 2\,\overline{\frac{u'v'}{u^2}} + \overline{\left(\frac{v'}{u}\right)^2}\right]$$

From equations (2) and (6b)

$$\overline{e_2^2} = \frac{S_2^2}{4}\left[\overline{\left(\frac{u'}{u}\right)^2} - 2\,\overline{\frac{u'v'}{u^2}} + \overline{\left(\frac{v'}{u}\right)^2}\right]$$

From equations (2) and (6a) and (6b)

$$4\overline{(e_1 + e_2)^2} = \overline{\left(S_1\frac{dU_1}{U_1} + S_2\frac{dU_2}{U_2}\right)^2} = (S_1 + S_2)^2\overline{\left(\frac{u'}{u}\right)^2} + (S_1^2 - S_2^2)2\,\overline{\frac{u'v'}{u^2}} + (S_1 - S_2)^2\overline{\left(\frac{v'}{u}\right)^2}$$

$$4\overline{(e_1 - e_2)^2} = \overline{\left(S_1\frac{dU_1}{U_1} - S_2\frac{dU_2}{U_2}\right)^2} = (S_1 - S_2)^2\overline{\left(\frac{u'}{u}\right)^2} + (S_1^2 - S_2^2)2\,\overline{\frac{u'v'}{u^2}} + (S_1 + S_2)^2\overline{\left(\frac{v'}{u}\right)^2}$$

In terms of equation (3), these become

$$D^2\gamma_1 = \frac{S_1^2}{4}\left[\overline{\left(\frac{u'}{u}\right)^2} + 2\,\overline{\frac{u'v'}{u^2}} + \overline{\left(\frac{v'}{u}\right)^2}\right] \tag{7}$$

$$D^2\gamma_2 = \frac{S_2^2}{4}\left[\overline{\left(\frac{u'}{u}\right)^2} - 2\,\overline{\frac{u'v'}{u^2}} + \overline{\left(\frac{v'}{u}\right)^2}\right] \tag{8}$$

$$4D^2\gamma_{1+2} = (S_1 + S_2)^2\overline{\left(\frac{u'}{u}\right)^2} + (S_1^2 - S_2^2)2\,\overline{\frac{u'v'}{u^2}} + (S_1 - S_2)^2\overline{\left(\frac{v'}{u}\right)^2} \tag{9}$$

$$4D^2\gamma_{1-2} = (S_1 - S_2)^2\overline{\left(\frac{u'}{u}\right)^2} + (S_1^2 - S_2^2)2\,\overline{\frac{u'v'}{u^2}} + (S_1 + S_2)^2\overline{\left(\frac{v'}{u}\right)^2} \tag{10}$$

From equations (7) and (8),

$$4D^2\left(\frac{\gamma_1}{S_1^2}+\frac{\gamma_2}{S_2^2}\right) = 2\left[\overline{\left(\frac{u'}{u}\right)^2}+\overline{\left(\frac{v'}{u}\right)^2}\right] \tag{11}$$

and

$$\frac{4D^2}{S_1S_2}(\gamma_1+\gamma_2) = \frac{S_1^2+S_2^2}{S_1S_2}\left[\overline{\left(\frac{u'}{u}\right)^2}+\overline{\left(\frac{v'}{u}\right)^2}\right]+2\left(\frac{S_1^2-S_2^2}{S_1S_2}\right)\frac{\overline{u'v'}}{u^2} \tag{12}$$

From equation (10)

$$\frac{4D^2}{S_1S_2}(\gamma_{1-2}) = \frac{S_1^2+S_2^2}{S_1S_2}\left[\overline{\left(\frac{u'}{u}\right)^2}+\overline{\left(\frac{v'}{u}\right)^2}\right]+2\left(\frac{S_1^2-S_2^2}{S_1S_2}\right)\frac{\overline{u'v'}}{u^2}-2\left[\overline{\left(\frac{u'}{u}\right)^2}-\overline{\left(\frac{v'}{u}\right)^2}\right] \tag{13}$$

Subtracting equation (13) from equation (12) leaves

$$\frac{4D^2}{S_1S_2}(\gamma_1+\gamma_2-\gamma_{1-2}) = 2\left[\overline{\left(\frac{u'}{u}\right)^2}-\overline{\left(\frac{v'}{u}\right)^2}\right] \tag{14}$$

Adding equations (11) and (14) yields

$$\frac{4D^2}{S_1S_2}\left[\frac{S_2}{S_1}\gamma_1+\frac{S_1}{S_2}\gamma_2+\gamma_1+\gamma_2-\gamma_{1-2}\right] = 4\overline{\left(\frac{u'}{u}\right)^2}$$

By subtracting equation (14) from equation (11),

$$\frac{4D^2}{S_1S_2}\left[\frac{S_2}{S_1}\gamma_1+\frac{S_1}{S_2}\gamma_2-(\gamma_1+\gamma_2-\gamma_{1-2})\right] = 4\overline{\left(\frac{v'}{u}\right)^2}$$

and when equation (8) is subtracted from equation (7),

$$D^2\left(\frac{\gamma_1}{S_1^2}-\frac{\gamma_2}{S_1^2}\right) = \frac{\overline{u'v'}}{u^2}$$

Let $\left(\frac{S_1}{S_2}\right)^2\frac{\gamma_2}{\gamma_1} = \zeta$, and $\frac{S_1}{S_2}\left(1+\frac{\gamma_2}{\gamma_1}-\frac{\gamma_{1-2}}{\gamma_1}\right) = a$; then these three equations become

$$\overline{\left(\frac{u'}{u}\right)^2} = D^2 \frac{\gamma_1}{S_1^2} (1 + \zeta + a) \tag{15}$$

$$\overline{\left(\frac{v'}{u}\right)^2} = D^2 \frac{\gamma_1}{S_1^2} (1 + \zeta - a) \tag{16}$$

$$\frac{\overline{u'v'}}{u^2} = D^2 \frac{\gamma_1}{S_1^2} (1 - \zeta) \tag{17}$$

And the correlation coefficient is

$$\frac{\overline{u'v'}}{\sqrt{\overline{u'^2}}\sqrt{\overline{v'^2}}} = \frac{1 - \zeta}{\sqrt{(1 + \zeta + a)(1 + \zeta - a)}} = \frac{1 - \zeta}{1 + \zeta}\sqrt{\frac{1}{1 - \left(\frac{a}{1 + \zeta}\right)^2}} \tag{18}$$

The relation $\gamma_{1+2} + \gamma_{1-2} = 2(\gamma_1 + \gamma_2)$ gives alternate forms of the equations.

In the case in which α is not 45°,

$$\overline{\left(\frac{u'}{u}\right)^2} \quad \text{and} \quad \frac{\overline{u'v'}}{\sqrt{\overline{u'^2}}\sqrt{\overline{v'^2}}}$$

remain the same, but

$$\overline{\left(\frac{v'}{u}\right)^2} = D^2 \frac{\gamma_1}{S_1^2} (1 + \zeta - a) \tan^2 \alpha \tag{19}$$

$$\frac{\overline{u'v'}}{u^2} = D^2 \frac{\gamma_1}{S_1^2} (1 - \zeta) \tan \alpha \tag{20}$$

Equations (15), (19), and (20) were not used in calculating the results presented in this paper. It was found that the conventional direct methods of measuring u' and v' gave better results. Equation (18) has the advantage of containing only ratios of the wire sensitivities and thermogalvanometer readings; thus it minimizes the possible errors involved in the readings.

APPENDIX B

CALCULATION OF THE TURBULENT SHEAR DISTRIBUTION FROM VELOCITY PROFILE

Consider the boundary-layer form of the Navier-Stokes equation

$$u \frac{\partial u}{\partial x} + v \frac{\partial u}{\partial y} = \frac{1}{\rho} \frac{\partial \tau}{\partial y} \qquad (1)$$

Since it is known that the widths of the free turbulent mixing zones increase linearly with the axial distance, the following new independent variable can be introduced.

$$\xi = \sigma \frac{y}{x}$$

If a stream function of the form $\psi = \frac{A}{\sigma} xF(\xi)$ is chosen the two velocity components become

$$u = AF'(\xi)$$

$$v = \frac{A}{\sigma} [\xi F'(\xi) - F(\xi)]$$

By substituting these forms in equation (1),

$$-A^2 \frac{\xi}{x} F'F'' + A^2 F'' \frac{1}{x} (\xi F' - F) = \frac{\sigma}{\rho} \frac{B}{x} G'(\xi)$$

where $\tau = BG(\xi)$

or

$$-A^2 F''F = \frac{\sigma}{\rho} BG'$$

$$G = -\frac{A^2 \rho}{\sigma B} \int_{+\infty}^{\xi} F''F \, d\xi$$

$$-\frac{\sigma \tau}{A^2 \rho} = \int_{+\infty}^{\xi} F''F \, d\xi$$

In order to be able to carry out the integration graphically, the form of the integral has to be changed.

Assume $F' = 1 - f$. Then

$$\int_{+\infty}^{\xi} FF''\,d\xi = \left[FF' - \int F'^2\,d\xi\right]_{+\infty}^{\xi}$$

$$= \left[(1-f)\left(\int^{\xi}(1-f)d\xi + c\right) - \int (1-f)^2\,d\xi\right]_{+\infty}^{\xi}$$

$$= \left[(1-f)\int^{\xi}(1-f)d\xi + c(1-f) - \int d\xi + \int 2f\,d\xi - \int f^2\,d\xi\right]_{+\infty}^{\xi}$$

$$= -cf + \int_{+\infty}^{\xi}(f - f^2)d\xi - f\int^{\xi}(1-f)d\xi$$

where c is the constant of integration.

Hence,

$$-\frac{\sigma\tau}{\rho A^2} = -cf + \int_{+\infty}^{\xi}(f - f^2)d\xi - f\int^{\xi}(1-f)d\xi$$

From the boundary condition:

$$\tau = 0, \quad f = 1 \quad \text{for} \quad \xi = -\infty$$

Therefore,

$$c = \int_{+\infty}^{-\infty}(f - f^2)d\xi - \int^{-\infty}(1-f)d\xi$$

Thus, the dimensionless form of the turbulent shearing stress becomes

$$-\frac{\sigma\tau}{\rho A^2} = -f\int_{+\infty}^{-\infty}(f - f^2)d\xi + f\int_{\xi}^{-\infty}(1-f)d\xi + \int_{+\infty}^{\xi}(f - f^2)d\xi$$

REFERENCES

1. Lin, C. C.: On the Stability of Two-Dimensional Parallel Flows. Proc. Nat. Acad. Sci., Vol. 30, Oct. 1944, pp. 316-324.

2. Goldstein, S.: Modern Developments in Fluid Dynamics. Clarendon Press (Oxford), 1938.

3. von Kármán, Th.: Some Aspects of the Turbulence Problem. Proc. Fourth Int. Congress for Appl. Mech., 1934, pp. 54-91.

4. Taylor, G. I.: Some Recent Developments in the Study of Turbulence. Proc. Fifth Int. Congress for Appl. Mech., 1938, pp. 294-309.

5. Millikan, C. B.: A Critical Discussion of Turbulent Flow in Channels and Circular Tubes. Proc. Fifth Int. Congress for Appl. Mech., 1938, pp. 386-392.

6. von Mises, R.: Some Remarks on the Laws of Turbulent Motion in Tubes. Kármán Anniversary Volume, pp. 317-327.

7. Reichardt, H.: Gesetzmässigkeiten der freien Turbulenz. VDI Forschungsheft 414, vol. 13, 1942.

8. Squire, H. B.: Reconsideration of the Theory of Free Turbulence. Rep. No. Aero. 2023, March 1945.

9. Taylor, G. I.: Statistical Theory of Turbulence. Proc. Roy. Soc. London, ser. A, vol. 151, no. 873, Sept. 1935, pp. 421-478.

10. von Kármán, Th., and Howarth, L.: On the Statistical Theory of Isotropic Turbulence. Proc. Roy. Soc. London, ser. A, vol. 164, no. 917, Jan. 1938, pp. 192-215.

11. Chou, P. Y.: On an Extension of Reynolds' Method of Finding Apparent Stress and the Nature of Turbulence. Chinese Jour. of Physics, no. 4, Jan. 1940, pp. 1-33.

12. Görtler, H.: Berechnung von Aufgaben der freien Turbulenz auf Grund eines neuen Näherungsansatzes. Z.f.a.M.M., vol. 22, no. 5, Oct. 1942, pp. 244-254.

13. Loitsianskii, L. G.: Integral Methods in the Theory of the Boundary Layer. NACA TM No. 1070, 1944.

14. von Kármán, Th.: The Fundamentals of the Statistical Theory of Turbulence. Jour. Aero. Sci., vol. 4, no. 4, Feb. 1937, pp. 131-138.

15. Cordes, G.: Untersuchung zur statischen Druckmessung in turbulenter Strömung. Ing. Arch., vol. 8, no. 4, Aug. 1937, pp. 245-270.

16. Dryden, H. L.: Turbulence Investigation at the National Bureau of Standards. Proc. Fifth Int. Congress for Appl. Mech., 1938, pp. 366-368.

17. Reichardt, H.: Messungen turbulenter schwankungen. Die Naturwissenschaften, no. 24/25, June 17, 1938, pp. 404-408.

18. Tollmien, Walter: Calculation of Turbulent Expansion Processes. NACA TM No. 1085, 1945.

19. Betz, A.: Velocity and Pressure Distribution behind Bodies in an Air Current. NACA TM No. 268, 1924.

20. Corrsin, S.: Investigation of Flow in an Axially Symmetrical Heated Jet of Air. NACA ACR No. 3L23, 1943.

21. Dryden, H. L., and Kuethe, A. M.: The Measurement of Fluctuations of Air Speed by the Hot-Wire Anemometer. NACA Rep. No. 320, 1929, p.7.

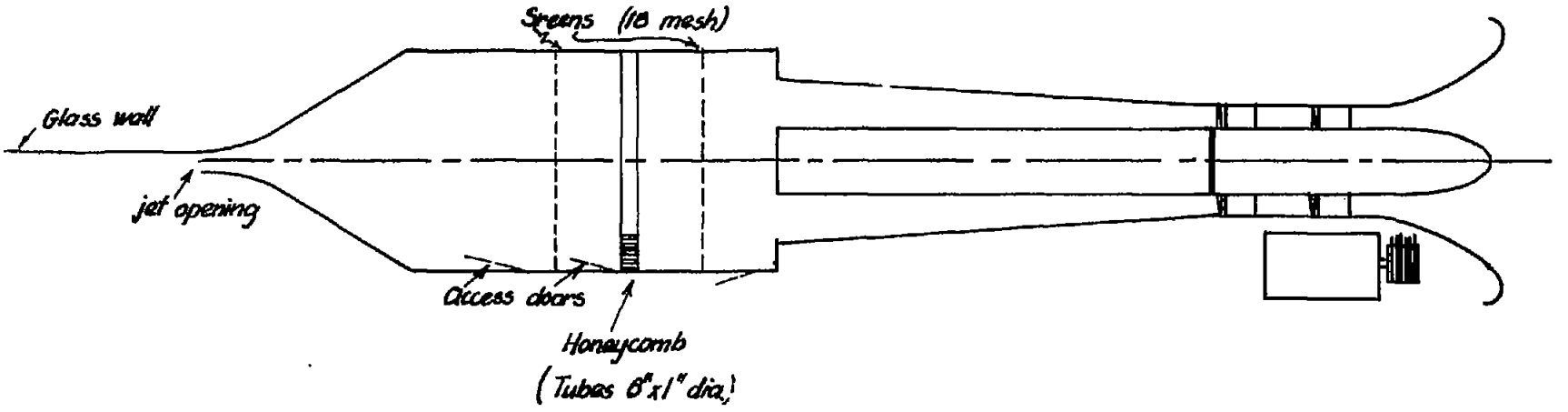

NATIONAL ADVISORY COMMITTEE
FOR AERONAUTICS

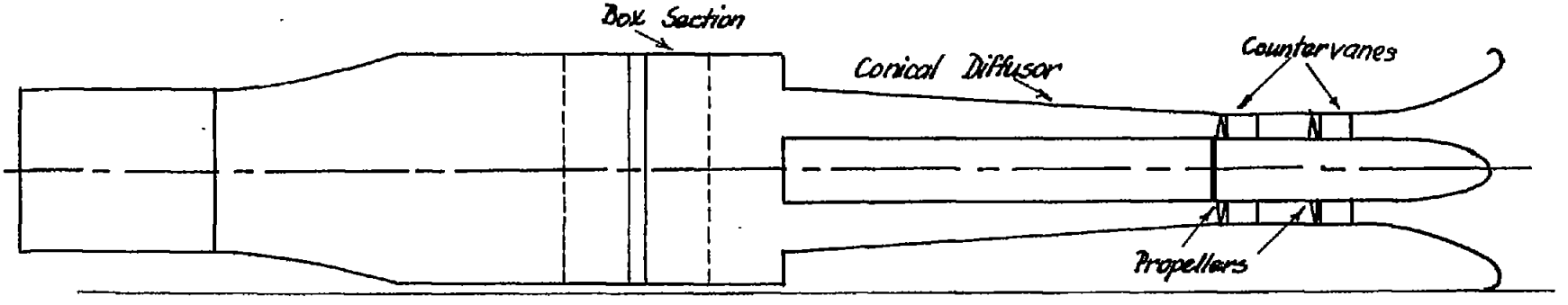

Figure 1.- Flow diagram of the two-dimensional tunnel.

Scale: $\frac{3}{16}$" - 1'

WC-7

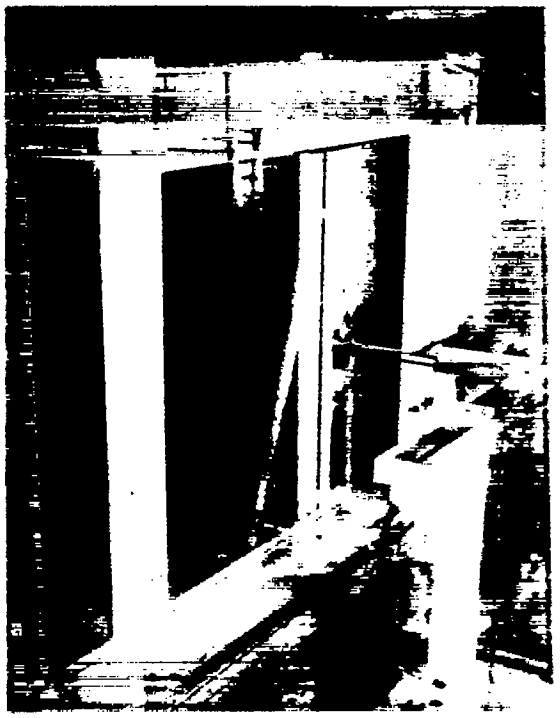

Figure 2.- Test section.

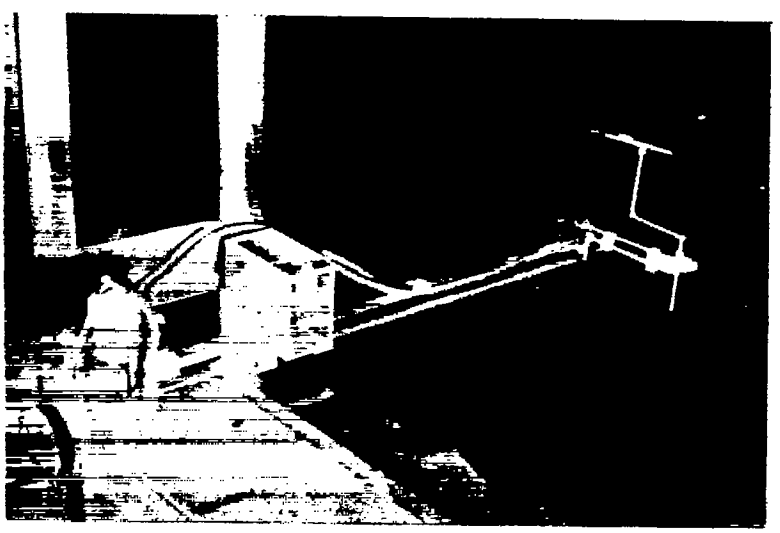

Figure 3.- Traversing mechanism.

NATIONAL ADVISORY COMMITTEE
FOR AERONAUTICS

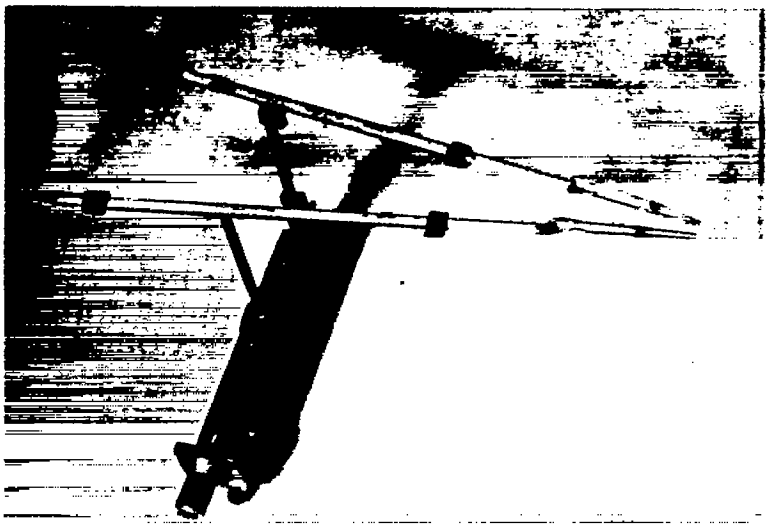

Figure 4.- Hot-wire carriage used for R_y measurements.

Figure 5.- Correlation figure at x = 54.3 centimeters, y/δ = 4.62.

Figure 6.- Correlation figure at x = 54.3 centimeters, y/δ = 3.72.

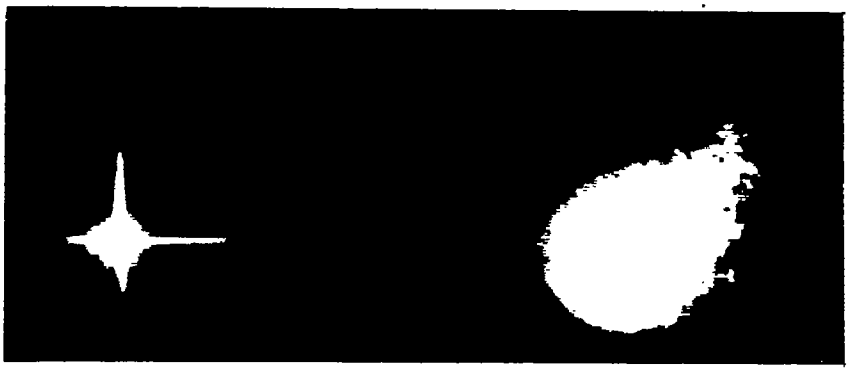

Figure 7.- Correlation figure at x = 54.3 centimeters, y/δ = 2.66.

Figure 8.- Correlation figure at x = 54.3 centimeters, y/δ = 2.05.

Figure 9.- Correlation figure at x = 54.3 centimeters, y/δ = 0.32.

Figure 10.- Correlation figure at x = 54.3 centimeters, y/δ = 0.64.

Figure 11.- Correlation figure at x = 54.3 centimeters, y/δ = 2.86.

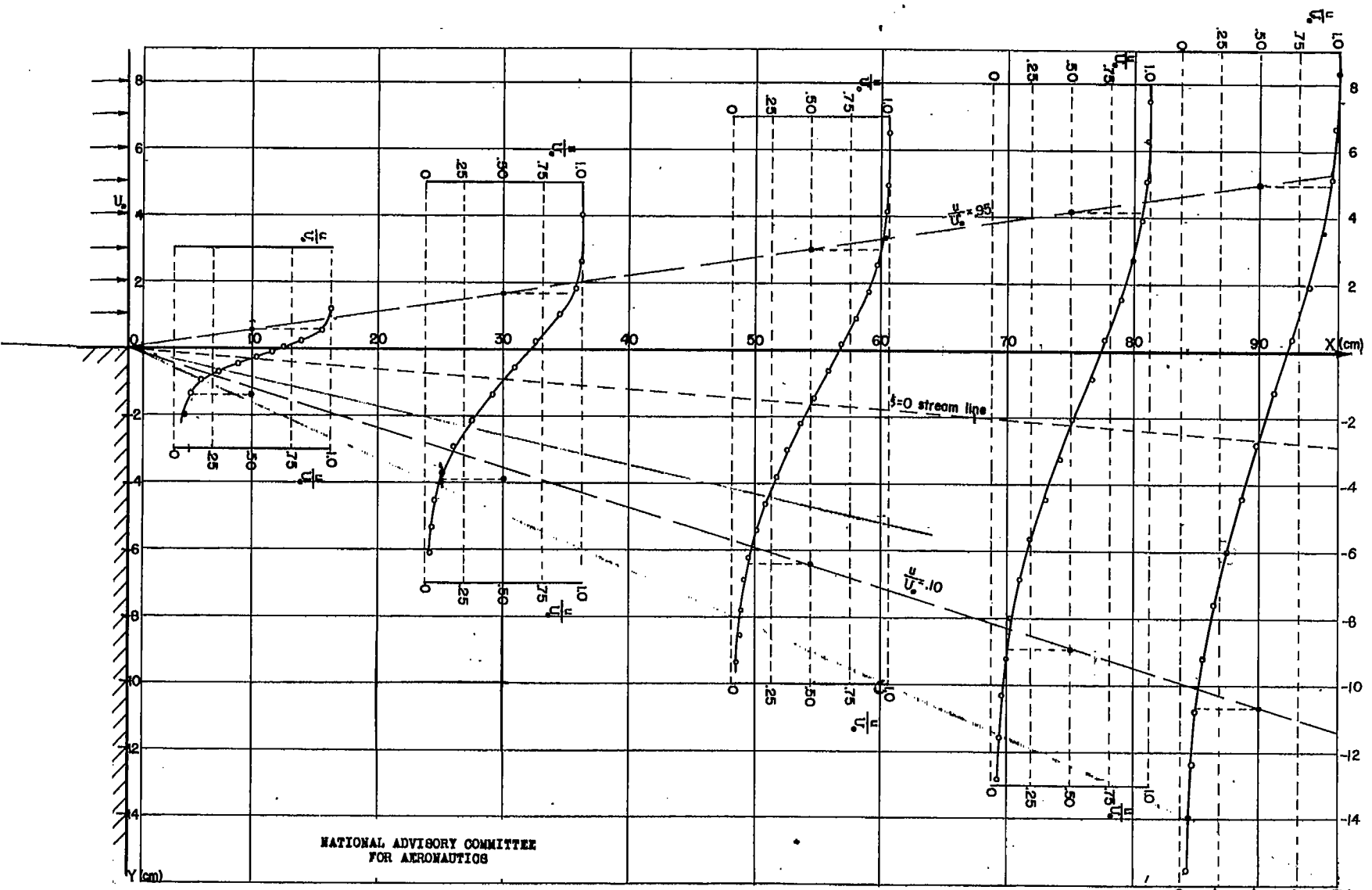

Figure 12.- Spread of the mean velocity in a two-dimensional half jet.

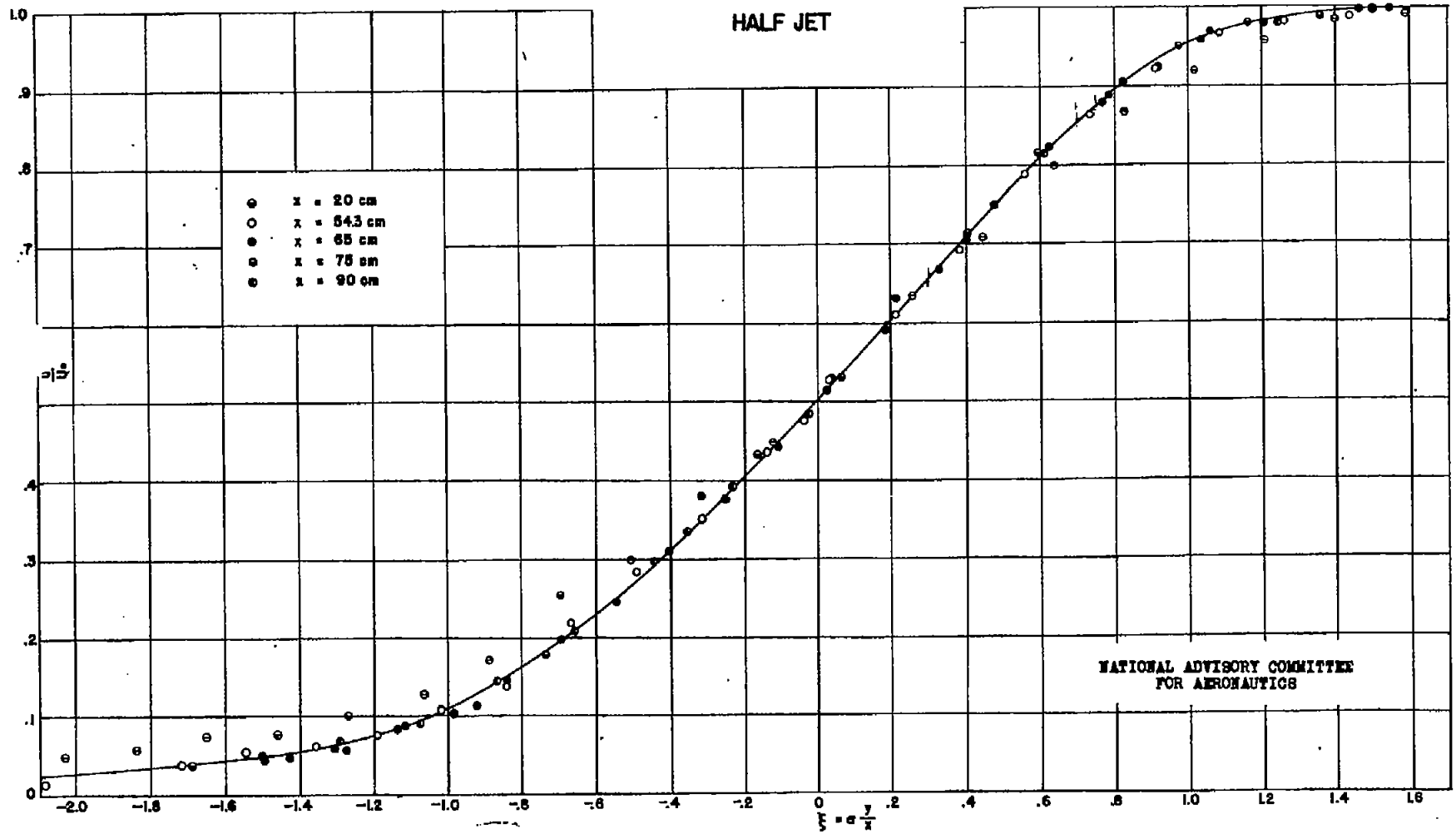

Figure 13.- Mean-velocity distributions (measured); $\sigma = 12.0$.

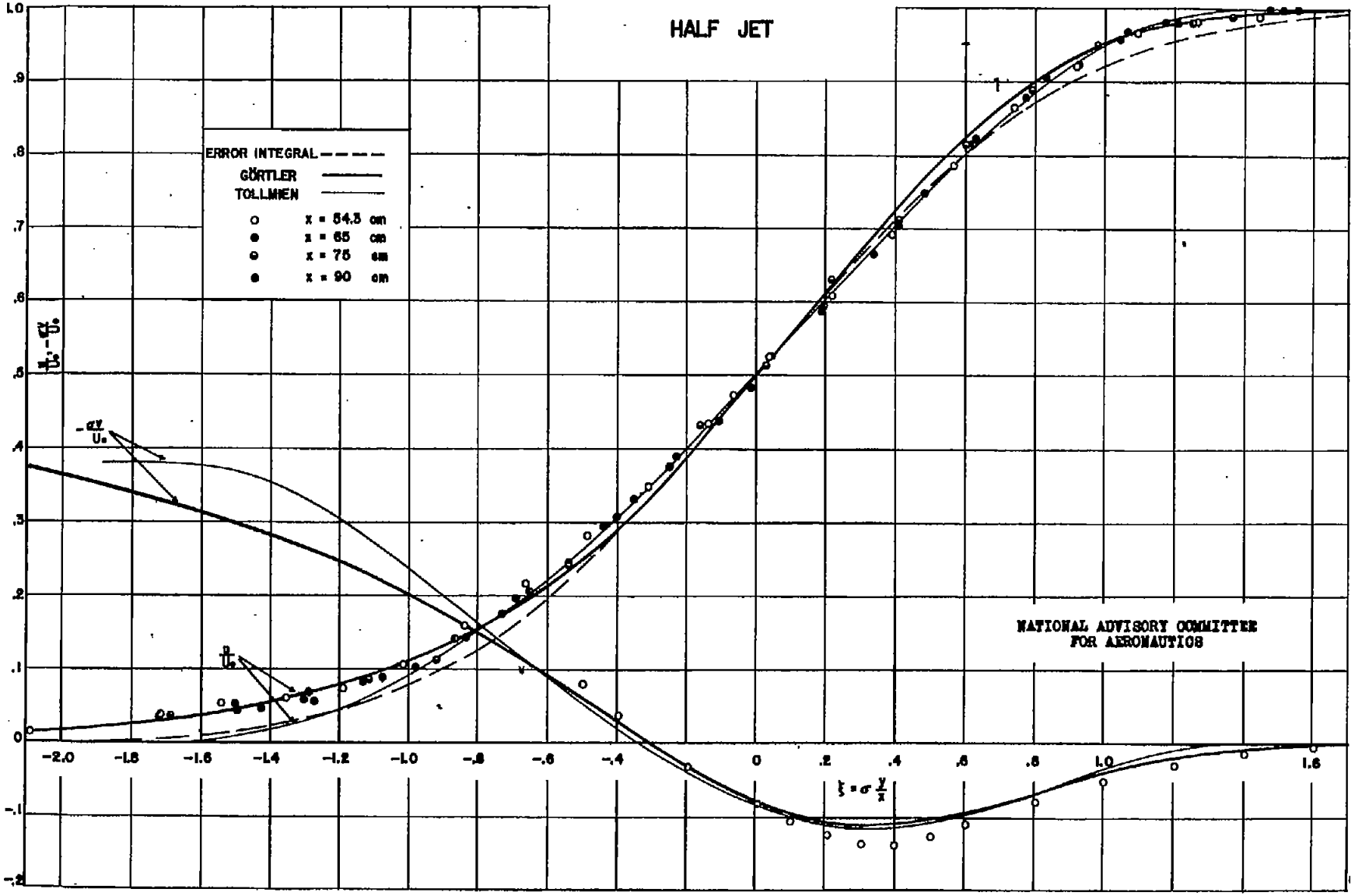

Figure 14.- Mean-velocity distributions (measured as compared with theoretical); $\sigma = 13.0$.

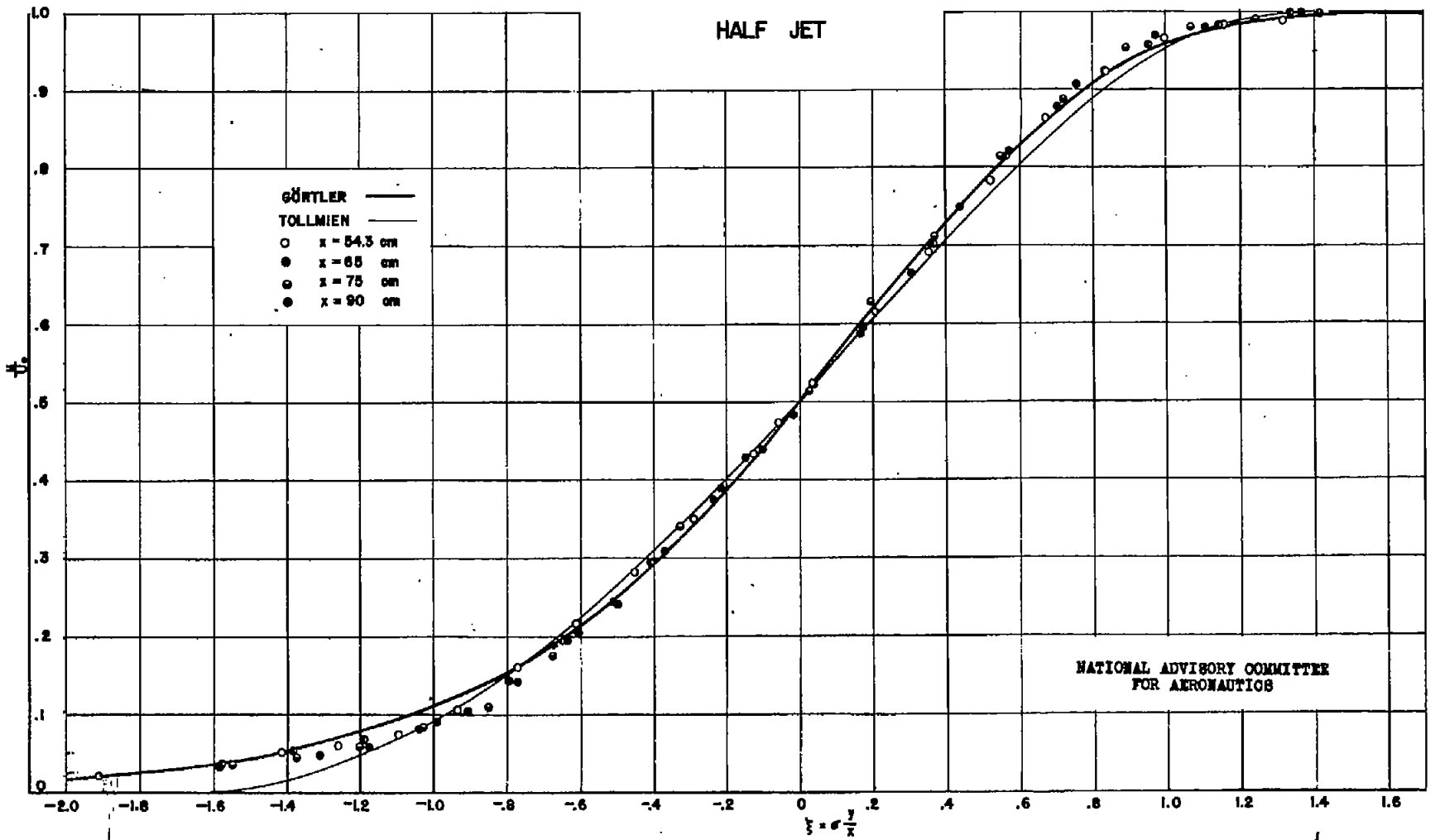

Figure 15.- Mean-velocity distributions (measured as compared with theoretical); $\sigma = 11.0$.

HALF JET

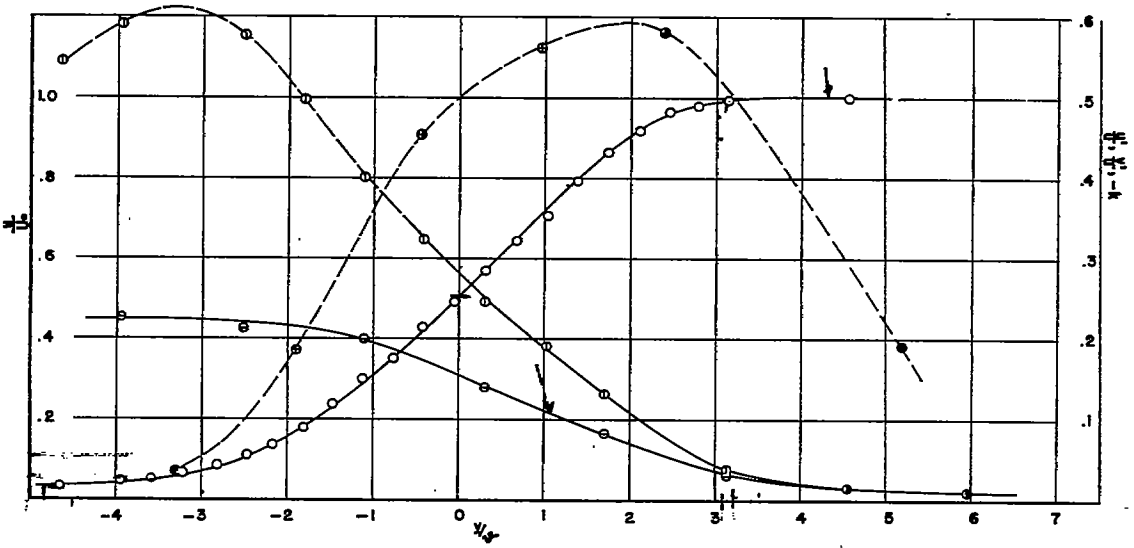

Figure 16.- Lateral distribution of mean and fluctuating velocities and correlation coefficient; x = 30 centimeters.

4.8 = 3.2

HALF JET

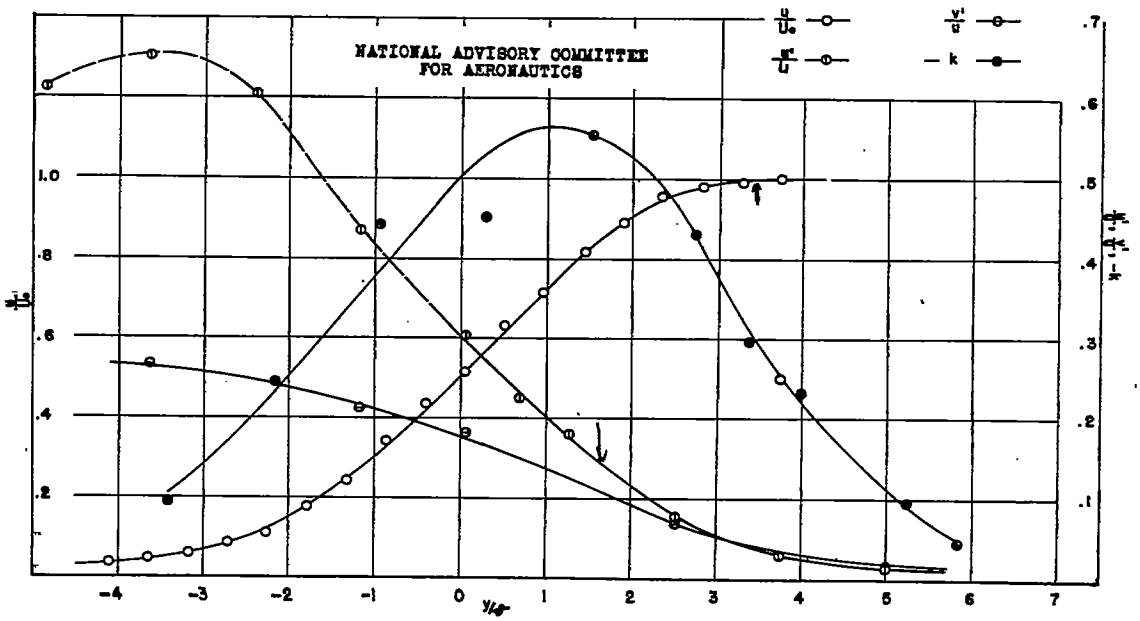

Figure 18.- Lateral distribution of mean and fluctuating velocities and correlation coefficient; x = 75 centimeters.

HALF JET

NATIONAL ADVISORY COMMITTEE
FOR AERONAUTICS

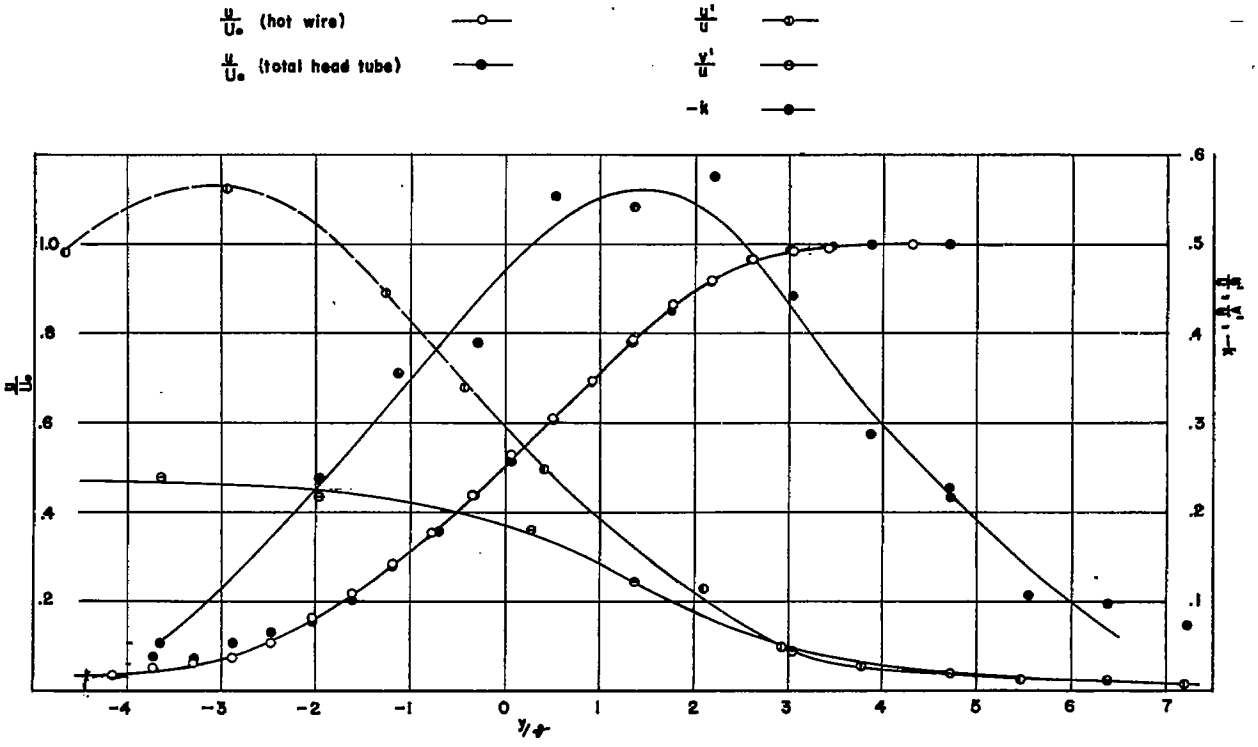

Figure 17.- Lateral distribution of mean and fluctuating velocities and correlation coefficient; x = 54.3 centimeters.

WC-7

HALF JET

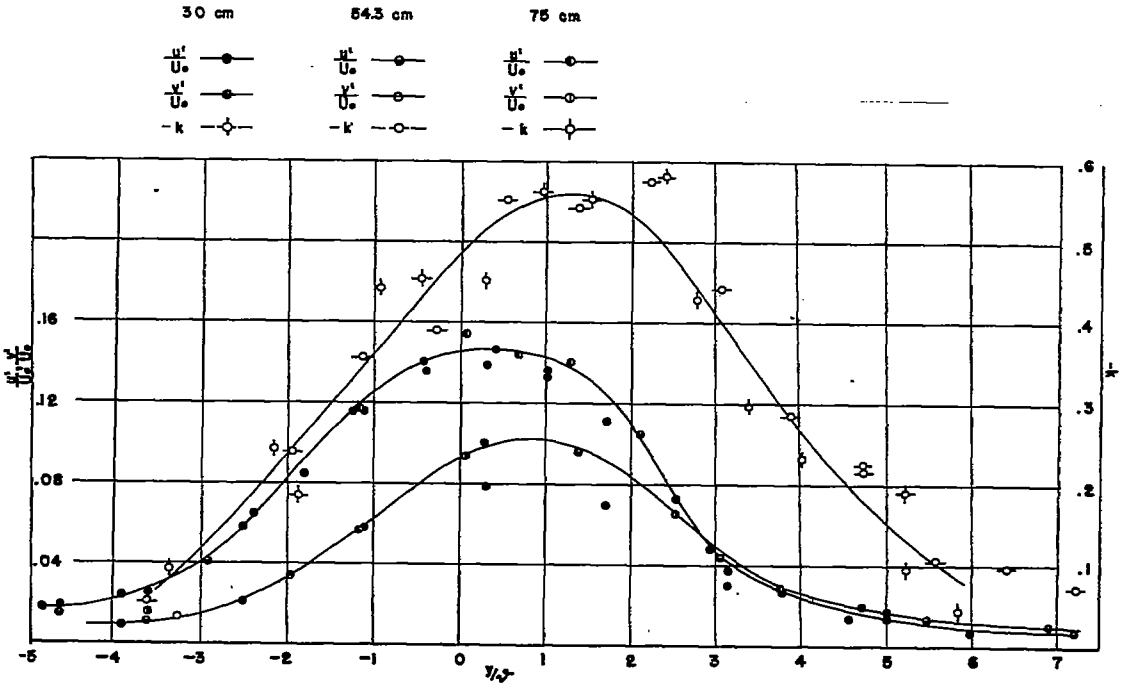

Figure 19.- Turbulence levels and correlation coefficient measured at three stations.

HALF JET

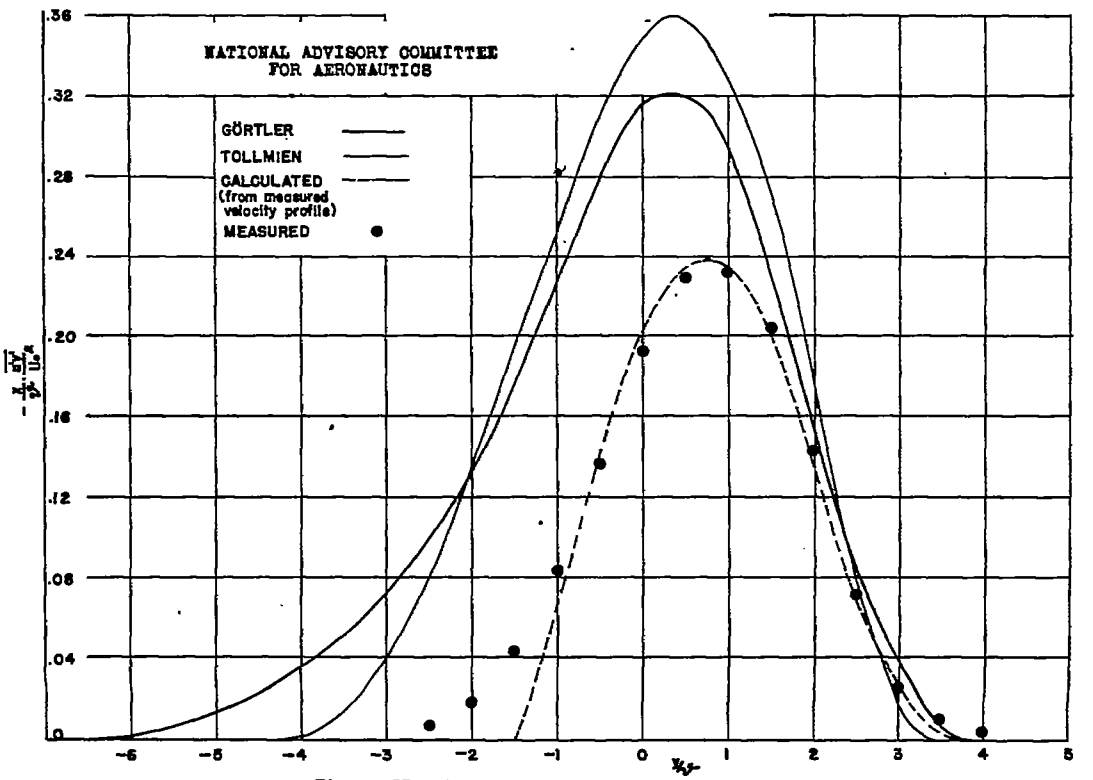

Figure 22.- Turbulent shear distribution.

WC-7

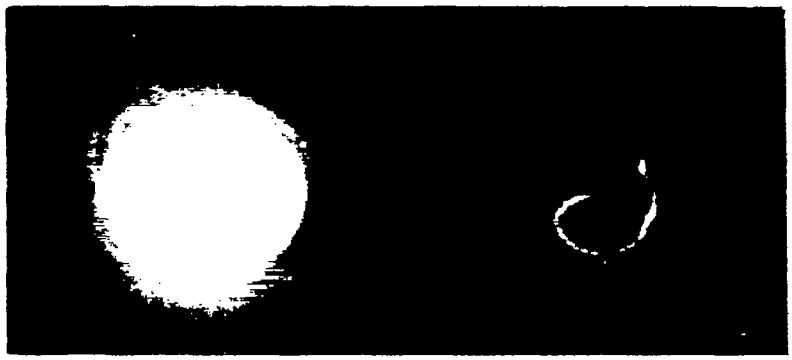

Figure 20.- Long and short time exposure of correlation figure in the free-stream side of the jet.

Figure 21.- Long and short time exposure of correlation figure behind a screen.

NATIONAL ADVISORY
COMMITTEE FOR AERONAUTICS

HALF JET

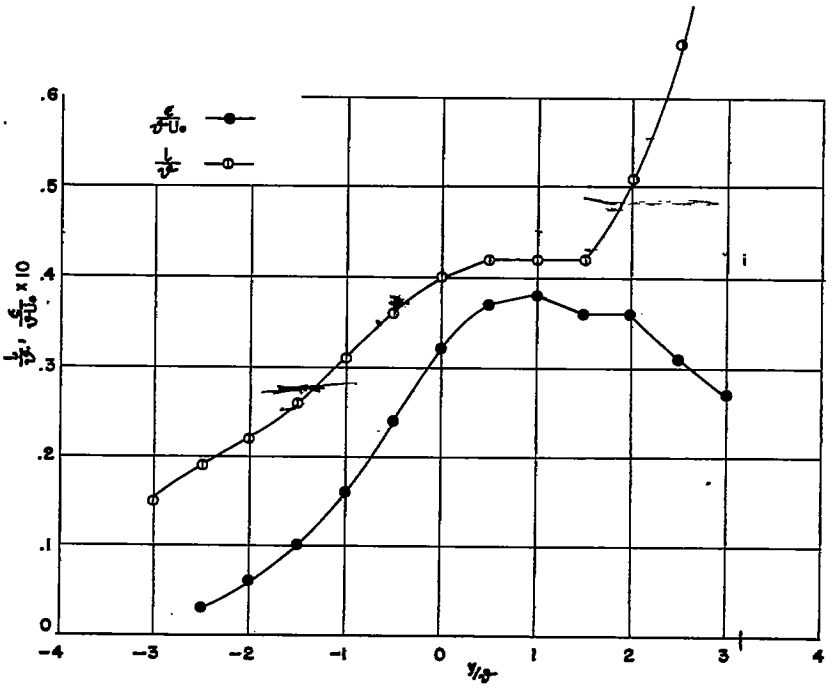

Figure 23.- Variation of exchange coefficient and mixing length across mixing zone.

HALF JET

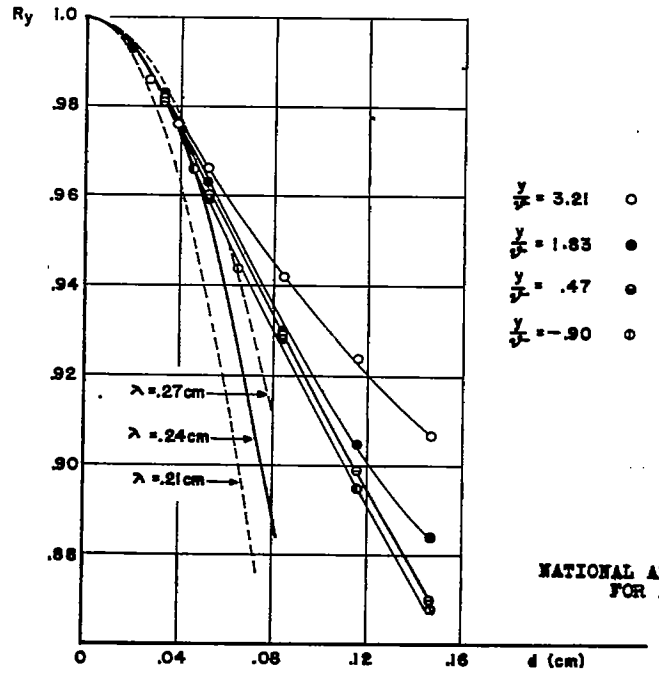

NATIONAL ADVISORY COMMITTEE FOR AERONAUTICS

Figure 24.- R_y distributions at different lateral positions; x = 30 centimeters.

HALF JET

NATIONAL ADVISORY COMMITTEE
FOR AERONAUTICS

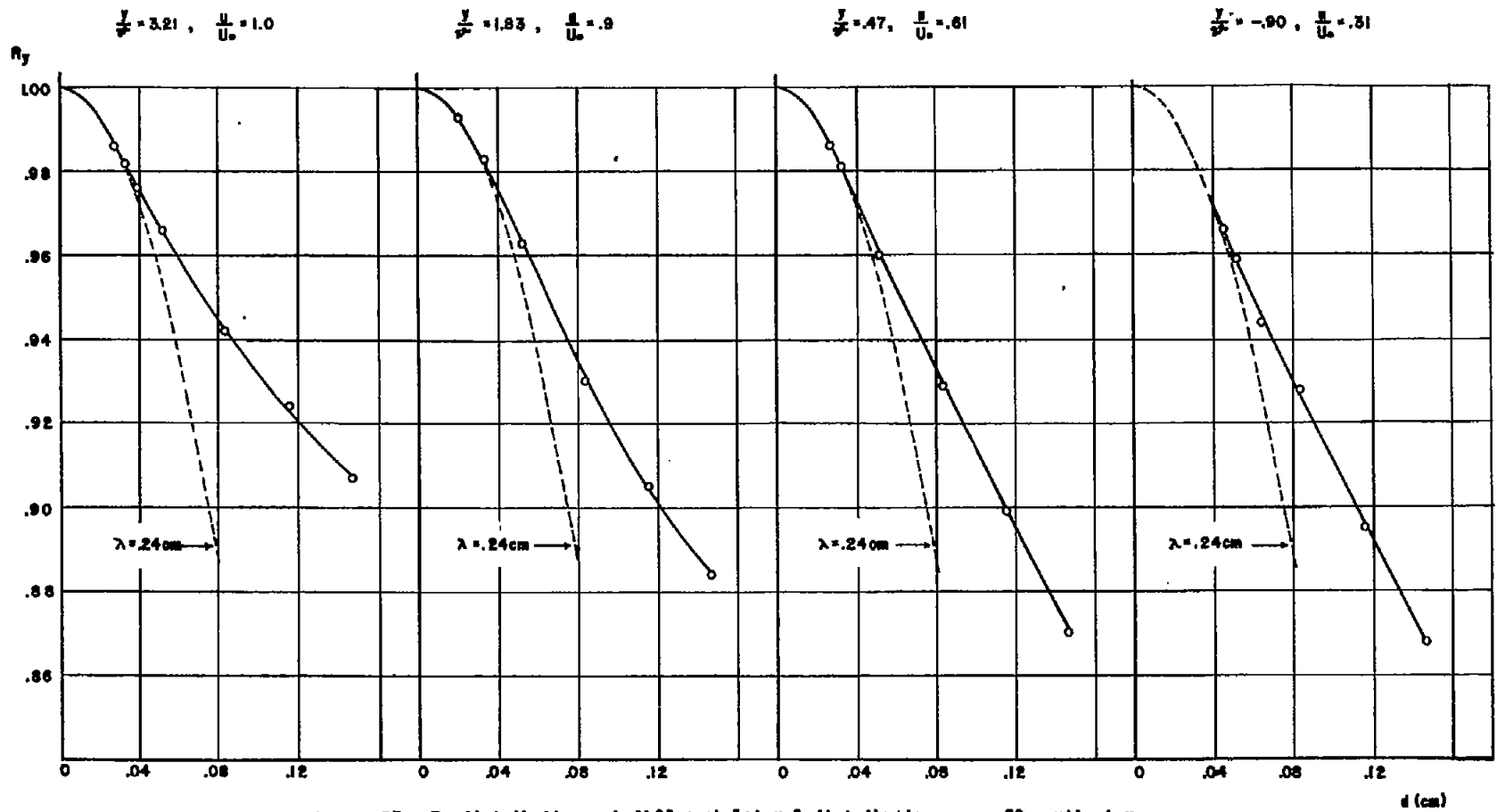

Figure 25.- R_y distributions at different lateral distributions; x = 30 centimeters.

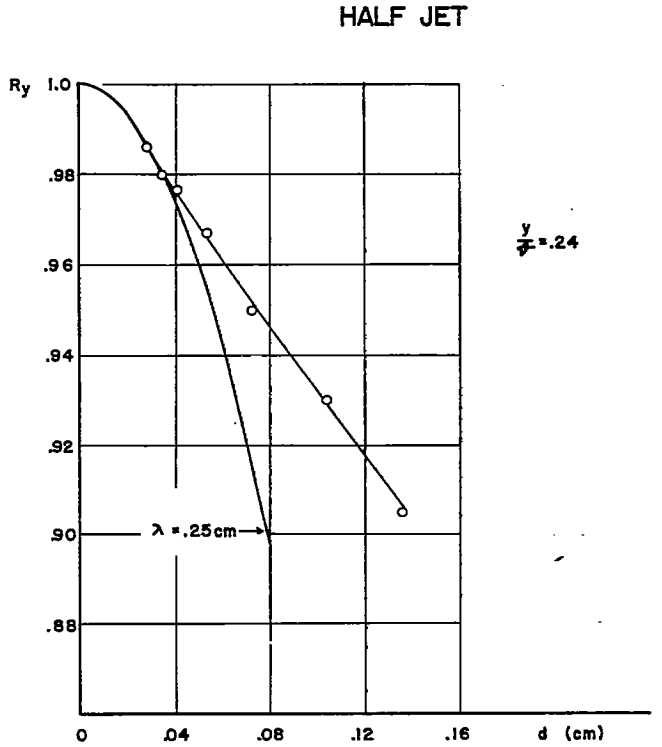

Figure 26.- R_y distributions at x = 40 centimeters.

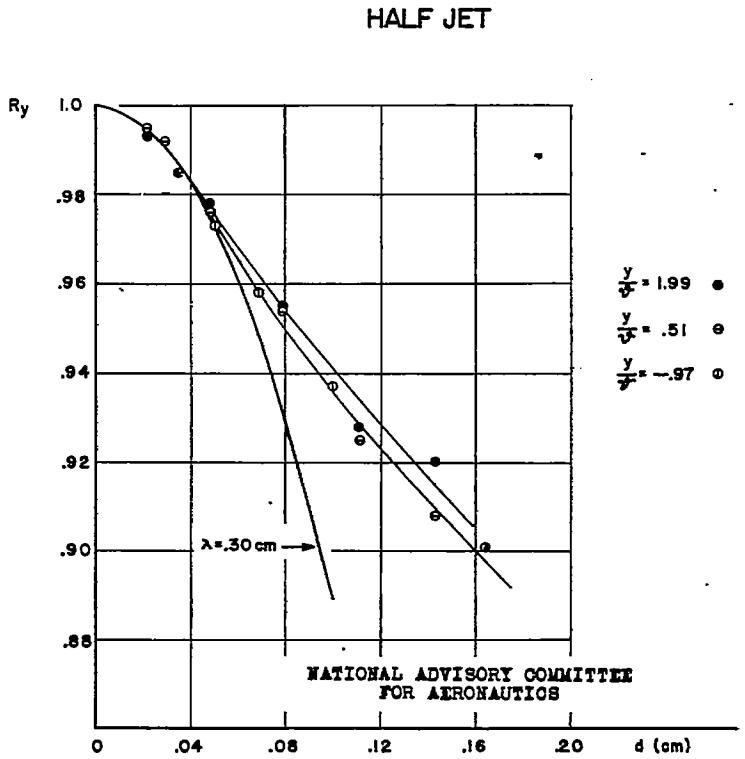

Figure 27.- R_y distributions at different lateral positions; x = 54.3 centimeters.

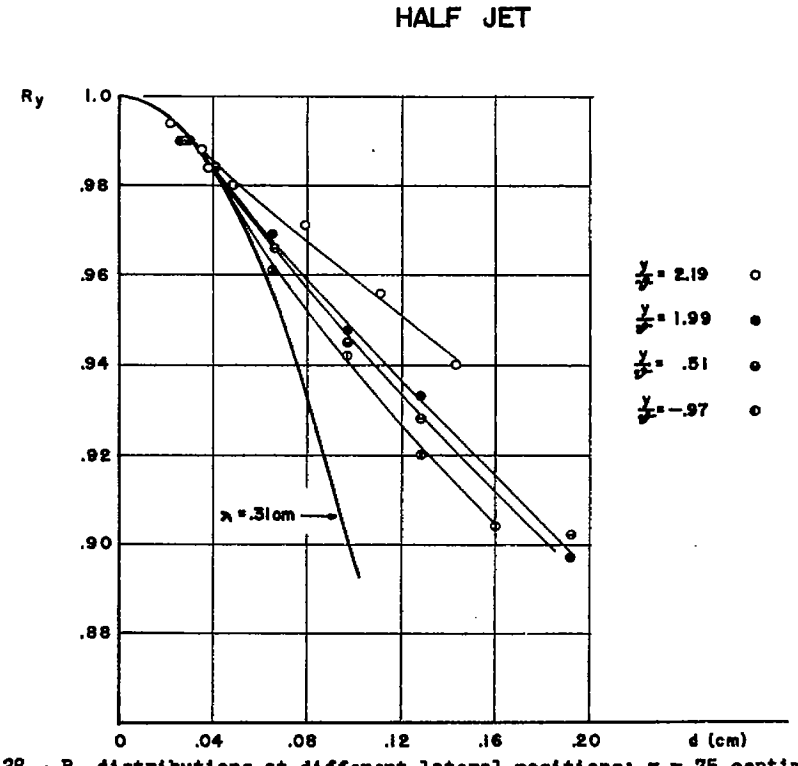

Figure 28.- R_y distributions at different lateral positions; x = 75 centimeters.

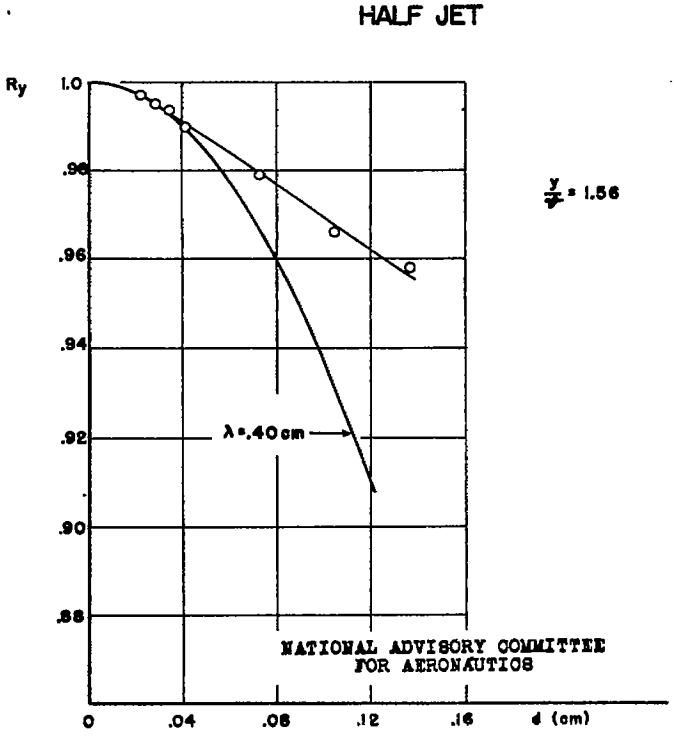

Figure 29.- R_y distribution at x = 80 centimeters.

HALF JET

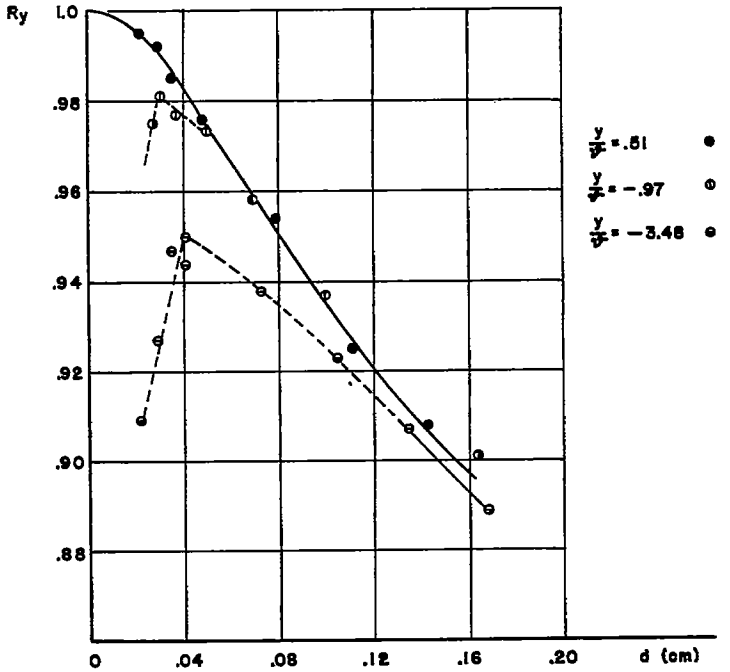

Figure 30.- Errors in measurements due to large fluctuations; x = 54.3 centimeters.

HALF JET

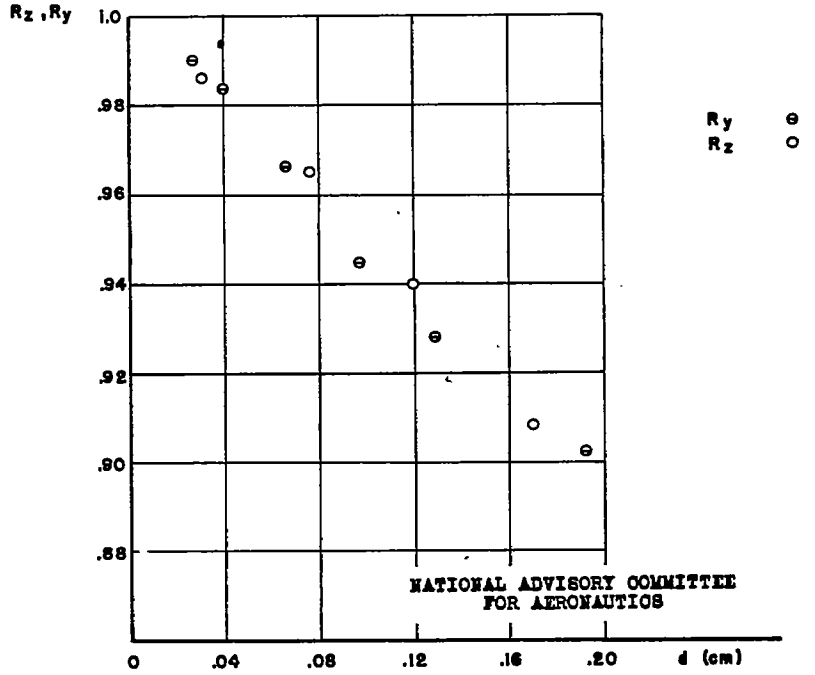

Figure 33.- Comparison of R_y and R_z measurements; x = 75 centimeters, y/b = 0.51.

Figure 31.- Long and short time exposure of R_y correlation at x = 75 centimeters, y/δ = 1.99 with d = 0.027 centimeter.

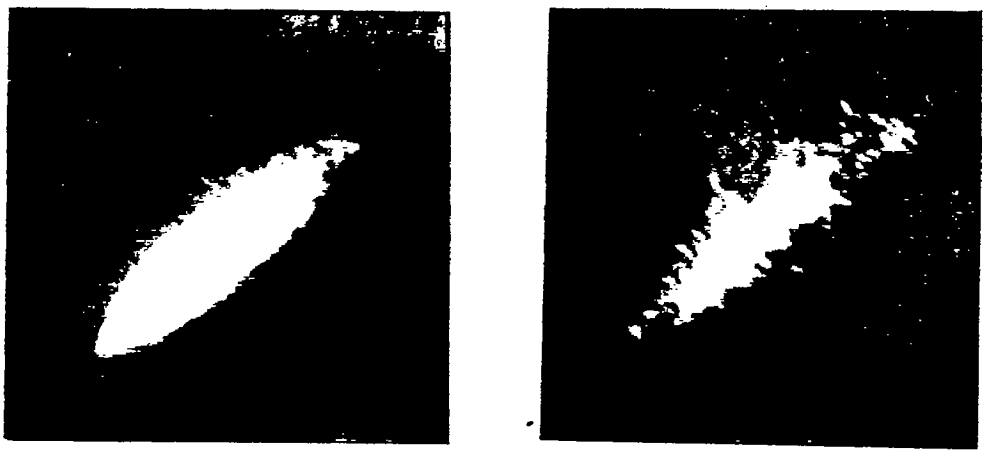

Figure 32.- Long and short time exposure of R_y correlation at x = 75 centimeters, y/δ = 1.99 with d = 0.192 centimeter.

HALF JET

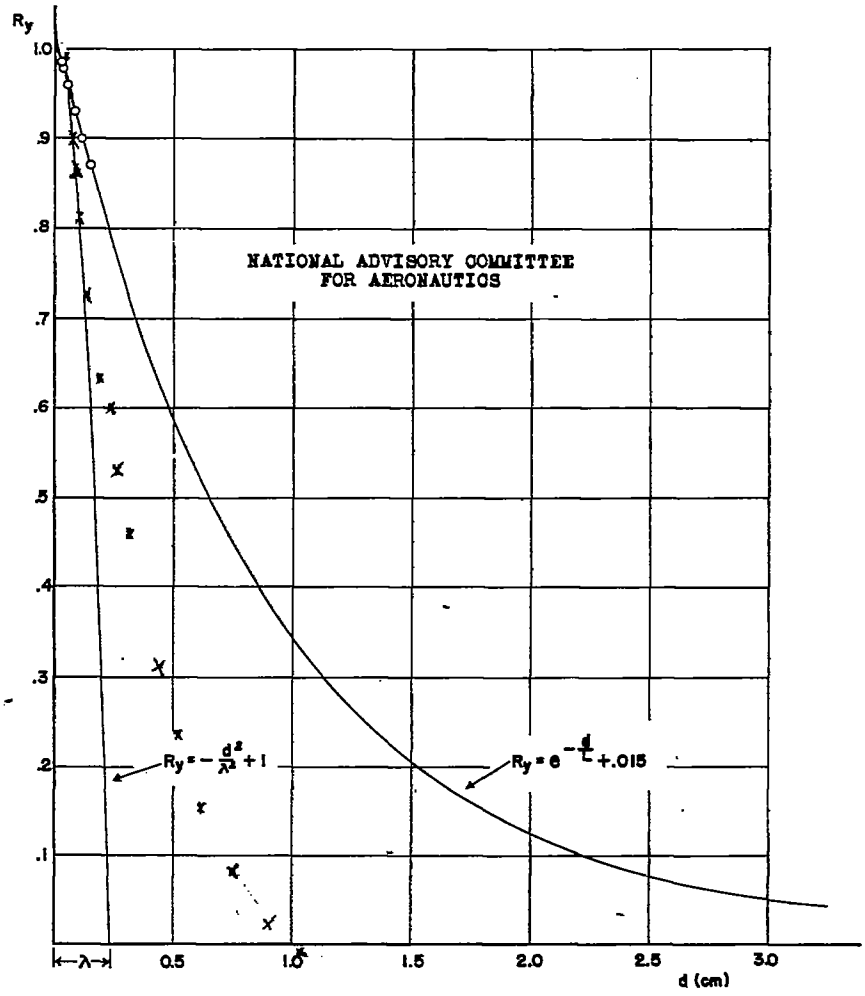

Figure 34.- R_y distribution at x = 30 centimeters, $y/\delta = 0.47$ indicating method of estimating the micro scale and scale of turbulence.

HALF JET

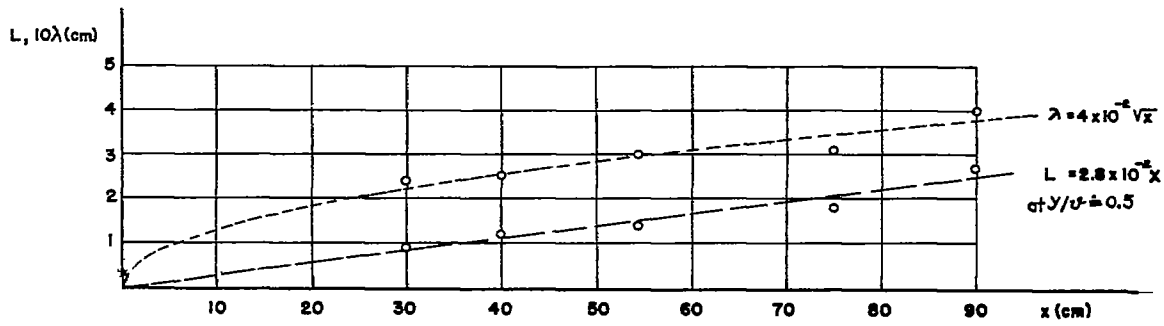

Figure 35.- Distribution of λ and L along the mixing zone.

HALF JET

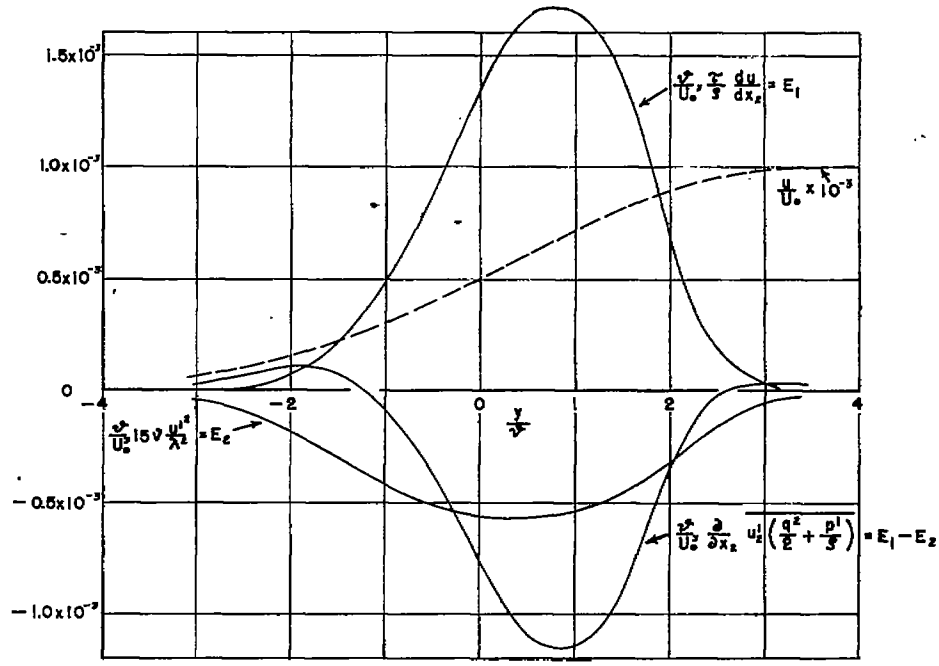

Figure 36.- Production, diffusion, and dissipation of turbulent energy across the mixing region.

HALF JET

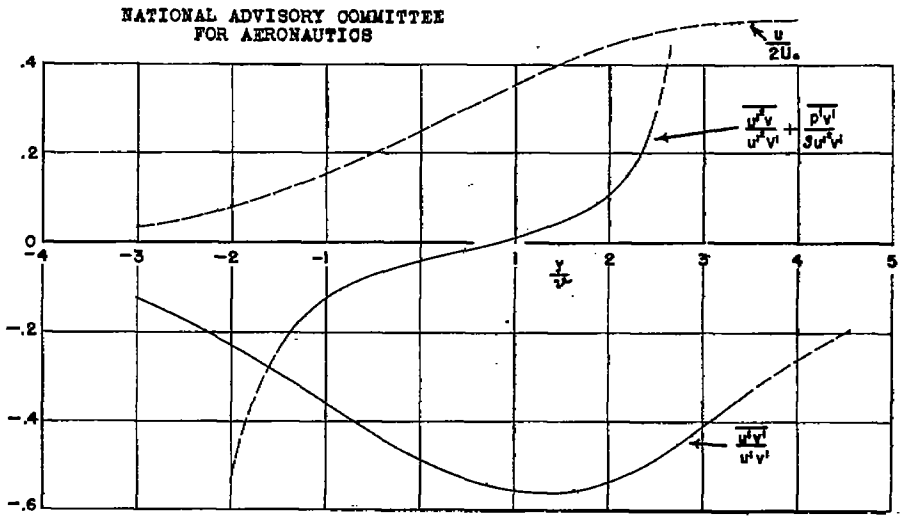

Figure 37.- Distribution of double and triple correlation coefficient across the mixing zone.